TECHNICAL MEMORANDUM

600

Estimates of spatial and inter-channel observation error characteristics for current sounder radiances for NWP

Niels Bormann, Andrew Collard and Peter Bauer

Research Department

October 2009

European Centre for Medium-Range Weather Forecasts
Europäisches Zentrum für mittelfristige Wettervorhersage
Centre européen pour les prévisions météorologiques à moyen terme

Series: ECMWF Technical Memoranda

A full list of ECMWF Publications can be found on our web site under:
http://www.ecmwf.int/publications/

Contact: library@ecmwf.int

European Centre for Medium-Range Weather Forecasts
Shinfield Park, Reading, RG2 9AX, England

Abstract

This paper uses three methods to estimate and examine observation errors and their correlations for clear-sky sounder radiances used in the ECMWF assimilation system. The study considers sounder-radiances from the main instruments currently in use, ie., AMSU-A, HIRS, MHS, AIRS, and IASI. The analysis is based on covariances derived from pairs of First Guess and analysis departures. The methods used are the so-called Hollingsworth/Lönnberg method, a method based on subtracting a scaled version of mapped assumed background errors from FG-departure covariances, and the Desroziers diagnostic.

The findings suggest that mid-tropospheric to stratospheric temperature sounding channels for AIRS and IASI and all AMSU-A sounding channels show little or no inter-channel or spatial observation error correlations, and estimates for the observation error are close to the instrument noise. Channels with stronger sensitivity to the surface show larger observation errors compared to the instrument noise, and some of this error is correlated spatially and between channels. Short-wave infrared temperature sounding channels also appear more prone to spatial observation error correlations. The three methods show good consistency for these estimates.

Estimating observation errors for humidity sounding channels appears more difficult. A considerable proportion of the observation error for humidity sounding channels appears correlated spatially for short separation distances, as well as between channels. Observation error estimates for humidity channels are generally considerably larger than those provided by the instrument noise.

Our statistics suggest that assumed background errors for tropospheric temperature are inflated (by about 30-60%), whereas there is little indication for background error inflation for stratospheric temperatures.

1 Introduction

In this paper we estimate and examine observation errors and their correlations for clear-sky radiances used in the ECMWF system. The assumed observation error covariance, together with assumed background error covariances, play an important role in determining the weight of a given observation in data assimilation systems. For technical or computational reasons, observation error covariance matrices used in data assimilation systems are mostly assumed to be diagonal.

Satellite radiances currently provide the largest input to today's data assimilation systems, both in terms of numbers and forecast impact, but the assumption of uncorrelated error is questionable for these observations. This is true for spatial as well as inter-channel error correlations. Observation errors used in data assimilation include errors from the observation operator, and radiative transfer models are likely to exhibit correlated errors, for instance due to errors in the spectroscopy or in the assumed gas concentrations (e.g., Sherlock 2000). Other aspects are also expected to lead to correlated observation errors, such as aspects of the instrument design or calibration, errors arising from the different representativeness of the radiances and the model fields, or even some common practices of quality control used in the assimilation system. Neglecting spatial error correlations in the assimilation can lead to sub-optimal analysis errors if the observations are used too densely (Liu and Rabier 2003).

While there is general agreement that radiances potentially have correlated observation errors, relatively few estimates of such error correlations are available, especially in the case of spatial error correlations. This is partly due to difficulties with the methods commonly used for such error estimation. A number of methods exist that are based on First Guess (FG) or analysis departures. Without further input, any such method can only be successful in separating FG errors and observation errors if the FG error and the observation error show sufficiently different characteristics (Dee and da Silva 1999). A commonly made assumption is that FG errors are spatially correlated, whereas observation errors are not. This is the basis of the so-called Hollingsworth/Lönnberg method (e.g., Hollingsworth and Lönnberg 1986, Rutherford 1972). This method has been applied by Garand

et al. (2007) who found considerable inter-channel radiance error correlations for AIRS data. The assumption of spatially uncorrelated observation error of course rules out any estimates for such errors, and it is questionable in the case of satellite radiances, as outlined above. Another method has recently been used to estimate observation error characteristics based on a consistency diagnostic summarised by Desroziers et al. (2005). The diagnostic can recover aspects of observation errors as long as the correlation scales of background and observation error are sufficiently different (e.g., Desroziers et al. 2009). The method has been applied to estimate variances of observation errors, as well as inter-channel error correlations (e.g., Menard et al. 2009, Stewart et al. 2009). As long as the length scales of FG and observation errors are sufficiently different, the diagnostic should be able to provide some estimates of spatial observation error correlations, but no attempts at calculating these are known to the authors.

Related methods have been developed for observation error tuning based on FG or analysis departure statistics, based on fitting an assumed model for the observation error correlations. Desroziers and Ivanov (2001) proposed a method to tune scaling coefficients for the observation error covariance matrix based on an optimality criterion for the cost function at the minimum, assuming the correlations are accurately represented in the initially assumed observation error covariance. This has been applied by Chapnick et al. (2006) and others for diagonal observation error covariance matrices. Related to this method is the maximum likelihood estimation (Dee and da Silva 1999) which directly fits free parameters of covariance models to FG-departure statistics. While these methods provide very useful tools, the drawback in our case is that little is known about what covariance models would be appropriate for inter-channel or spatial covariance models for satellite radiances. Using incorrect covariance methods (for instance, assuming uncorrelated observation error when error correlations are present in the real data) can lead to undesired results in these estimates (e.g., Liu and Rabier 2003, Chapnick et al. 2006). A less constrained characterisation of error correlations for radiance data is needed first.

Common methods to counteract spatial or inter-channel error correlations are spatial thinning or error inflation. Both are applied widely in data assimilation systems (e.g., Dando et al. 2007, Collard and McNally 2009). Guidance for selecting optimal thinning scales can be taken from Liu and Rabier (2003) who found that thinning scales of a threshold error correlation value of around 0.2 produced the smallest analysis error when error correlations are neglected and the diagonal observation errors are not inflated. However, since reliable estimates of spatial error correlations are lacking for radiance data, thinning scales currently used are mostly ad-hoc estimates.

In the present paper we provide estimates for observation errors and their inter-channel and spatial correlations for passive sounding instruments currently used in the ECMWF system. The aim is to provide guidance for the specification of observation error covariances and thinning scales in data assimilation. Given the difficulties of estimating observation errors, we employ three methods to better characterise the uncertainty inherent in these estimates. The data used for this study is described in the next section, followed by an overview of the methods employed. Next, the results are presented by instrument for the main radiance sounding instruments used in the ECMWF system and for estimates of scaling factors for the background errors. Finally, a discussion and conclusions are provided in the last section.

2 Data

We will investigate observation error covariances for sounder radiances currently assimilated operationally at ECMWF. This encompasses the following instruments: the Advanced Microwave Sounding Unit (AMSU)-A, the Microwave Humidity Sounder (MHS), the High Resolution Infrared Radiation Sounder (HIRS), Atmospheric Infrared Sounder (AIRS), and the Infrared Atmospheric Sounding Interferometer (IASI).

The statistics presented here are based on FG and analysis departures for pairs of observations. The obser-

vations in each pair are required to be less than 1 h apart (i.e., within one orbit) and originate from the same instrument on the same satellite. All possible pairs were collected over the chosen study period, and the pairs of observations were then binned by separation distance, using a binning interval of 25 km unless indicated otherwise. This allows one to calculate spatial covariance statistics as a function of separation distance. We mostly assume that the covariance statistics are isotropic. We also checked for departures from isotropy, and the results are presented where noteworthy departures from isotropy were found.

The departures were taken from the ECMWF system, using only data that was actively assimilated. We restrict ourselves to field-of-views (FOVs) for which all channels of an instrument are diagnosed as cloud free and pass further quality control checks. This is in contrast to the practice employed in the assimilation where the aim is to identify clear-sky channels rather than clear-sky FOVs. The reason for restricting ourselves to clear-sky FOVs is primarily to simplify the statistics and to harmonise the sampling for different channels in order to estimate inter-channel error correlations. The methods employed for cloud-screening are summarised in the results section for each instrument.

During the course of this study, we analysed departures taken from assimilation experiments performed for different periods, at different model resolution (ranging from T255 to T799), and with different thinning intervals (operational thinning and halved thinning interval). While some seasonal variations in the statistics exist, the overall results for the observation error covariance estimates were comparable for these variations, and differences were usually within the range of results from the three methods considered in this study. The results presented here are based on data for the 21-day period 22 August - 11 September 2008. The FG and analysis departures were taken from an assimilation experiment that used 4-dimensional variational data assimilation (4DVAR) with a 12-hour observation window, a model resolution of T799 ($\approx$ 25 km), an incremental analysis resolution of T255 ($\approx$ 80 km), and 91 levels in the vertical up to 0.01 hPa. The version of the assimilation system and the data selection was the same as that used in operations in April 2009, except that the thinning scale was approximately halved for all radiance data in our experiment. For the results presented here, one radiance datum is selected per 60 km box for each instrument where data is available. This increases the sample size for our purposes, especially for small separation distances.

We use departure statistics after bias correction, as these are the departures that primarily influence or reflect the atmospheric analysis. The bias correction is performed within the analysis using variational bias correction (e.g., Dee 2004). Unless indicated otherwise, the bias correction uses a linear model for the airmass bias, with a constant component and four layer thicknesses calculated from the FG as predictors (1000-300 hPa, 200-50 hPa, 50-5 hPa, 10-1 hPa). Scanbiases are modelled through a 3rd-order polynomial in the scan-position. The bias correction will partly correct for errors in the radiative transfer, as these tend to introduce large-scale air-mass dependent biases (e.g., Bormann et al. 2009).

3 Methods

In the following, we describe the methods used in this paper to estimate the observation errors and their correlations. They are all based on the FG or analysis departure statistics from the database of pairs of observations introduced above. The observation error covariances are intended to be the sum of all errors relevant to the interpretation of the radiances in data assimilation. This includes instrument and calibration errors, errors of representativity (from the representation of different scales in the horizontal or vertical in the radiances and the model data), and errors in the observation operator (i.e., errors in the radiative transfer used to assimilate the radiances, such as errors in spectroscopy), as long as they have not been addressed by the bias correction. We will use the term “observation error” to refer to the diagonal of the observation error covariance matrix.

3.1 Hollingsworth/Lönnberg

This method is based on the assumption that true background errors are spatially correlated, whereas observation errors are spatially uncorrelated. As a result, observation errors can be estimated by calculating FG-departure covariances from pairs of FG-departures as a function of separation distance. Observation errors are estimated by extrapolating the covariance/separation relationship from non-zero separations to zero-separation, so that the FG-departure variance at zero separation is split into a spatially correlated part and a spatially uncorrelated component. The latter is assumed to represent primarily observation error. The method also assumes that observation and background errors are uncorrelated. The method has been applied numerous times to estimate background errors from FG-departures of radiosonde networks (e.g., Hollingsworth and Lönnberg 1986, Rutherford 1972), or, more recently, errors and inter-channel error correlations for AIRS radiances (Garand et al. 2007). A variant of the method has also been used to estimate spatial error correlations in Atmospheric Motion Vectors (AMVs) from differences between AMVs and radiosondes (Bormann et al. 2003). This variant is not well-suited to radiance data, as standard radiosonde observations do not usually reach high enough in the atmosphere to perform the necessary radiative transfer calculations. More details on the Hollingsworth/Lönnberg method can be found in the above references. The method will be used here to estimate observation errors and inter-channel error correlations.

To perform the extrapolation to zero distance from non-zero separations, a correlation function is frequently fitted to the covariance statistics as a function of separation distance for non-zero separations. For most data considered in this paper, the shortest separation distances are fairly small compared to length-scales of background error correlations. Instead of employing such a correlation function we therefore subtract the FG-departure covariance at the first sufficiently populated non-zero separation bin from the one for zero separation. We found this to produce more robust results, as the use of a correlation function gives results that are highly dependent on the choice of correlation function. The first sufficiently populated separation bin is typically in the range of 12.5 - 50 km, and the actual choice is stated by instrument in the results section. As FG-departure covariances tend to increase with decreasing separation, neglecting the use of a correlation function introduces an underestimation of the spatially correlated part of the FG-departure variances, and hence an overestimation of the observation error. On the other hand, the presence of any spatially correlated observation error will lead to an underestimation of the observation error, as such spatial correlations are neglected.

The assumption that observation errors are spatially uncorrelated is questionable in the case of satellite radiances. Here, the observation error includes the radiative transfer error, and it is expected that this error is spatially correlated, as errors in the spectroscopy or the assumed concentrations of atmospheric gases will be similar for neighbouring observations. Also, aspects of quality control, such as cloud screening, may lead to spatially correlated error. However, Garand et al. (2007) argue that such radiative transfer or screening errors are reduced through the bias correction. Nevertheless, it should be kept in mind that the Hollingsworth/Lönnberg method will only be able to estimate the spatially uncorrelated part of the observation error, and the results will be questionable if there are indications of significant spatial observation error correlations.

3.2 Background error method

This method uses covariances of FG-departures and subtracts from these the assumed background errors, mapped into radiance space. The background error estimates are taken from the assimilation system, and they have been derived using the ensemble method as described in Fisher (2003). The background-error-subtraction method assumes that observation and background errors are uncorrelated, and that the assumed background errors provide good estimates of the true background errors. The method is applied here to derive spatial as well as inter-channel observation error-characteristics.

The spatial and inter-channel background error characteristics in radiance space were calculated from an ensemble of 50 random perturbations to short-term forecast fields, with perturbations consistent with the assumed background error characteristics. These global perturbations were calculated at a horizontal truncation of T255, consistent with the incremental analysis resolution of the assimilation system configuration used in this study. The perturbations were calculated for the 12-hour analysis cycle for 1 September 2009 00 Z, in the middle of our study period. The perturbations were mapped from the analysis variables into radiance space using the tangent linear of the radiative transfer model, assuming nadir viewing conditions. The resulting radiance perturbations were sampled at the respective observation locations for the instruments used in this study. Inter-channel background error covariances and spatial background error covariances were derived from these perturbations in the same way as the FG-departure covariances introduced earlier.

Note that the mapped background errors will be hampered by an incomplete modelling of skin temperature errors for channels with strong sensitivity to the surface. Skin temperature is not an analysis variable in the ECMWF system. Over sea, skin temperatures are prescribed through a sea surface temperature analysis (Stark et al. 2007). For our background error computations we assumed an error of 0.4 K for the skin temperature error over sea, based on in-situ validation of the sea surface temperature analysis (Stark et al. 2007). This error is assumed to be spatially uncorrelated. This assumption is probably unrealistic, so the mapped background errors will show unrealistic spatial characteristics for channels with strong sensitivity to the surface. For the same reason, the method is not applied for such channels over land, where skin temperature errors are expected to be larger. More details are provided for the channels in question.

During the course of this work, spatial characteristics of the mapped assumed background errors indicated that the assumed background errors are too large or too small when compared with spatial FG-departure covariances for some channels. In cases where the spatial correlation structures appeared nevertheless consistent with FG-departure covariances, but only the magnitude appeared off, a channel-specific scaling factor was introduced to make FG-departure covariances and the mapped background errors more consistent for larger separation distances. The scaling factor was calculated from data over separation distances between 200 and 1200 km. The scaling was only performed when the mapped background error covariances were larger than the FG-departure covariances at larger separation distances. This is to avoid that the scaling masks indications of spatial observation error correlations.

Used with scaling, the method becomes an extension of the Hollingsworth/Lönnberg method: we assume that background errors dominate FG-departure covariances at larger separation distances, and use as correlation function the empirical relationship between mapped assumed background errors and separation distance. We therefore allow for some spatial observation error correlations at shorter distances by assuming that the spatial background error correlations follow this empirical relationship. In the following we will refer to the method simply as the background error method.

3.3 Desroziers diagnostic

Assuming that variational data assimilation schemes broadly follow linear estimation theory, consistency diagnostics can be derived for observation, background and analysis errors in observation space from FG and analysis departures. These diagnostics have been derived and summarised by Desroziers et al. (2005), and here we make use of the following relationships:

$$\tilde{\mathbf{R}} = E\left[\mathbf{d}_a\,\mathbf{d}_b^T\right] \tag{1}$$

$$\mathbf{H}\tilde{\mathbf{B}}\mathbf{H}^T = E\left[\mathbf{d}_b\,\mathbf{d}_b^T\right] - E\left[\mathbf{d}_a\,\mathbf{d}_b^T\right] \tag{2}$$

where $\tilde{\mathbf{R}}$ is the diagnosed observation error covariance matrix, $\tilde{\mathbf{B}}$ is the diagnosed background error covariance matrix, $\mathbf{H}$ is the linearised observation operator, $\mathbf{d}_b$ are the background departures of the observations, $\mathbf{d}_a$ are the analysis departures of the observations, and $E[\,]$ is the expectation operator. Apart from the usual assumptions on Gaussian errors and no error correlations between FG and observation, etc., the diagnostic expressions also assume that the weight given to the observations in the analysis is in agreement with the true error covariances.

While primarily introduced as a consistency diagnostic, Desroziers et al. (2005) argue that the diagnostic equations may be used to estimate improved versions of the background or observation error covariances. They point out that the diagnostic equations formulate a fixed-point problem, and the solution may be derived at iteratively by using the diagnosed values in a subsequent assimilation, which is then used again to calculate the diagnositics. The method has been used to estimate observation errors and inter-channel error correlations (e.g., Menard et al. 2009, Stewart et al. 2009). For a simple case, Desroziers et al. (2005) show that the method has the capability of retrieving spatial correlation structures of observation errors, even if the initial assumed observation error is uncorrelated. This is possible as long as the true background errors and the true observation errors have sufficiently different correlation structures. The applicability of the method and its properties in the case of estimating spatial observation error correlations in realistic assimilation systems is an area of active research.

In the current paper, we refer to the results of equations (1) and (2) as the Desroziers diagnostics, and we use the results as further estimates of improved observation or background errors. The method is used to obtain spatial as well as inter-channel error correlations. For the current paper, we do not use the diagnostic observation error characteristics in subsequent assimilations, ie., we show results only after one iteration of the tuning method suggested by Desroziers et al. (2005).

It should be noted here that all three methods assume that errors in the FG and observation errors are uncorrelated. The assumption, however, is not strictly true. Quality control based on FG-departures is likely to introduce apparent correlations between FG errors and observation errors. Representativeness errors in the observations are also likely to be correlated with FG errors. Nevertheless, such error correlations are assumed to be small.

For all three methods, biases have been removed for the statistics presented here, either through the variational bias correction or by subtracting a global mean of residual biases. While the variational bias correction will ensure that biases between the observations and analyses are close to zero, residual biases can occur between observations and the FG in cases where there is considerable bias in the forecast model. This is is the case, for instance, for some stratospheric channels or some water vapour channels. This aspect needs to be kept in mind when the results are considered for use in data assimilation systems, as such biases may warrant adjustments to the observation errors that can be used in data assimilation.

4 Results

In the following, we present the results of our analysis for the five instruments considered here. Unless indicated otherwise, statistics are shown for data over sea. Results for data over land are also shown for surface-sensitive channels if any are used for the particular instrument.

4.1 AMSU-A

AMSU-A is a 15-channel cross-track scanning microwave radiometer, primarily designed to sound atmospheric temperature in the 50 GHz oxygen band (e.g., Goodrum et al. 2009). It provides data sampled at 48 km across-

track and 52.7 km along-track resolution at nadir. We discuss statistics for the NOAA-18 AMSU-A, as it is considered the best AMSU-A in orbit at the moment. Channels 5-14 are considered for assimilation at ECMWF, with channel 5 and 6 rejected over land over higher orography. Lower tropospheric channels are rejected over sea when the First Guess (FG)-departure for channel 3 exceeds 3 K to avoid regions with a strong cloud or rain signal (a FG-departure threshold of 0.7 K on channel 4 departures is used over land). Additional checks for scattering signatures are also performed. The outermost three scan positions of each scanline are rejected (out of 30 scan positions). Channel 14 is used without bias correction to anchor the stratospheric temperature analysis.

4.1.1 General results

Figure 1 shows covariance statistics for the FG departures for used NOAA-18 AMSU-A data (diagonal only) as a function of separation distance. They show sizeable differences between the covariance values at zero-separation and those at non-zero separation, and the expected reduction of covariance values with separation

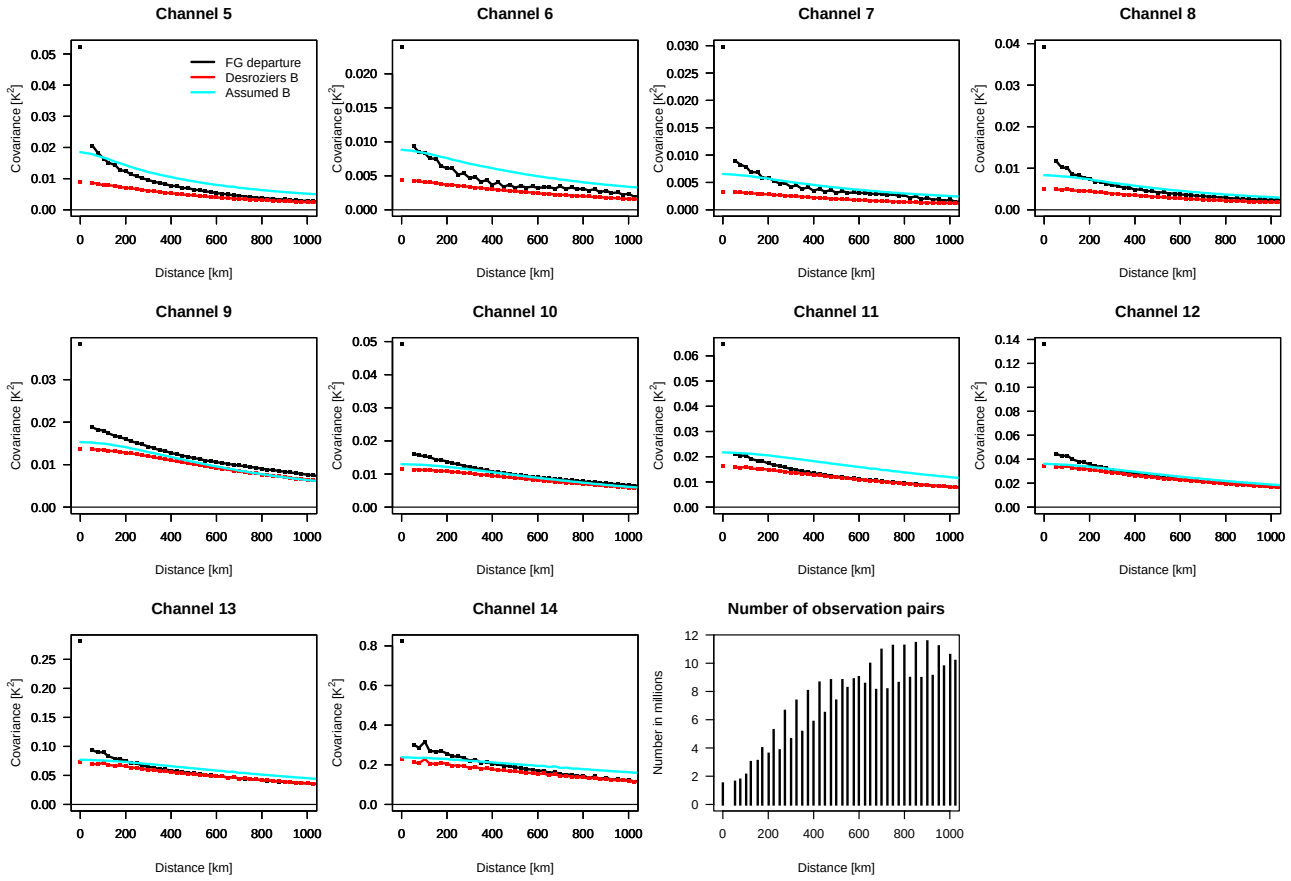

Figure 1: First Guess departure covariances (black), Desroziers' background error diagnostic (red), and mapped background error covariance (cyan) as a function of separation distance for the NOAA-18 AMSU-A channels used in the ECMWF system. The number of collocations as a function of separation distance is shown in the last panel; the spikes in the number of pairs for certain separation distances are due to moiré effects from the binning interval and the AMSU-A sampling grid. Separation bins with fewer than 5000 observations are not shown.

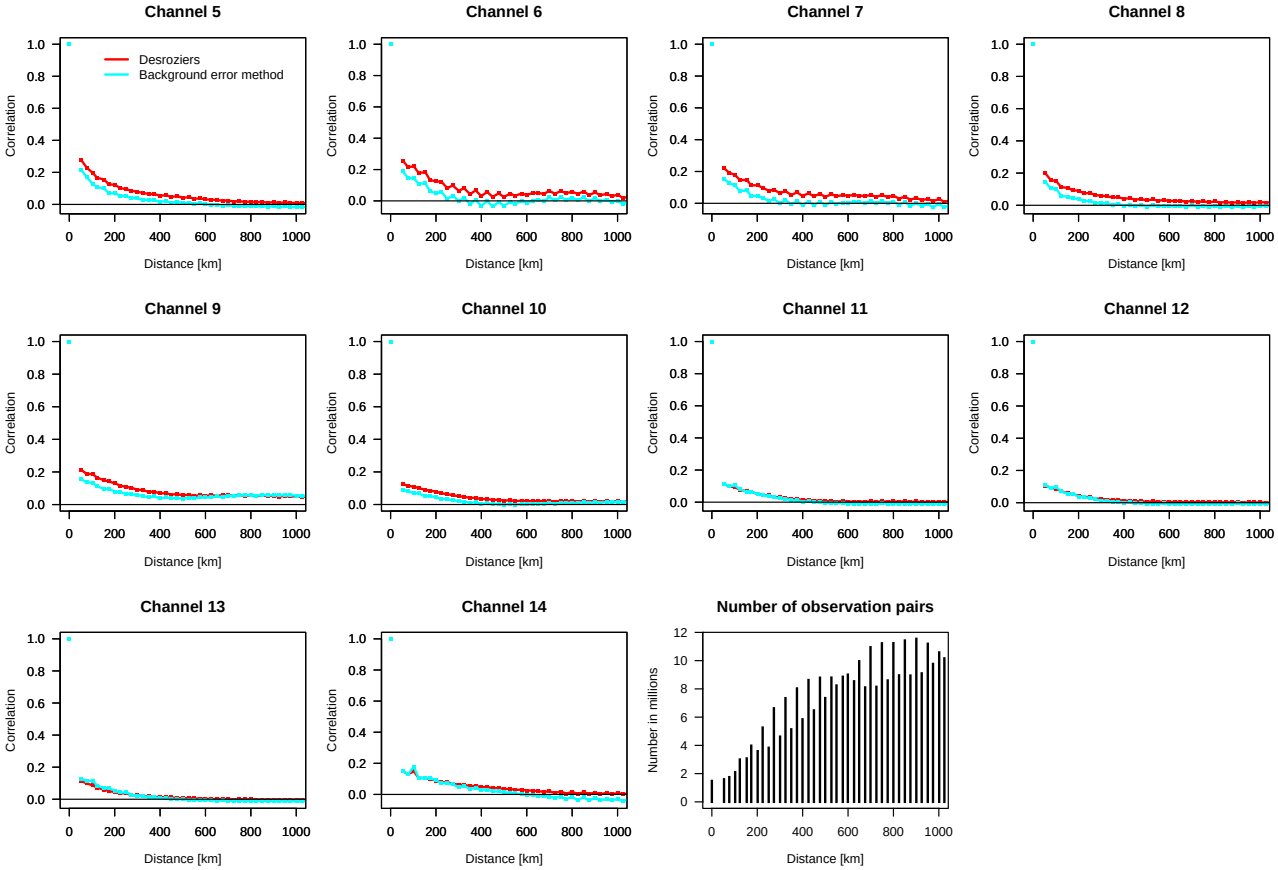

Figure 2: Estimates of spatial error correlations as a function of separation distance for NOAA-18 AMSU-A for the channels used at ECMWF. The estimates are based on Desroziers' diagnostic (red) and the background error method (cyan). The number of collocations as a function of separation distance is shown in the last panel.

distance. Given the size of the difference between zero-separation and non-zero separation and the fact that errors in the FG will be spatially correlated, it is already aparent that the spatially uncorrelated part of the observation error for AMSU-A dominates.

The FG-departure statistics are shown together with characteristics calculated from the assumed background error statistics, and the diagnostic for the background error given by Desroziers (equation 2). For channels 5-8, 11, and 13-14, the sampled background error statistics are somewhat larger than the covariances calculated from the FG-departures for separations greater than 200-300 km. This suggests that the assumed background errors are either larger than the true background errors or that the average spatial characteristics of the assumed background error in radiance space are not consistent with observations. The Desroziers-estimated background errors are, by defintion, smaller than the covariances from the FG-departures. While this means they are also considerably smaller than the assumed background errors, the shape of the reduction with separation distance is actually fairly similar. It is therefore likely that the assumed background errors are in fact inflated for the channels in question, whereas the spatial characteristics are consistent with observations. For channels 9, 10, and 12, the Desroziers-estimated background errors are very close to the sampled background errors.

Figure 2 shows estimates of the spatial error correlations for AMSU-A observations. One estimate is based on Desroziers' diagnostic (equation 1), whereas the other one is based on the background error method. Both

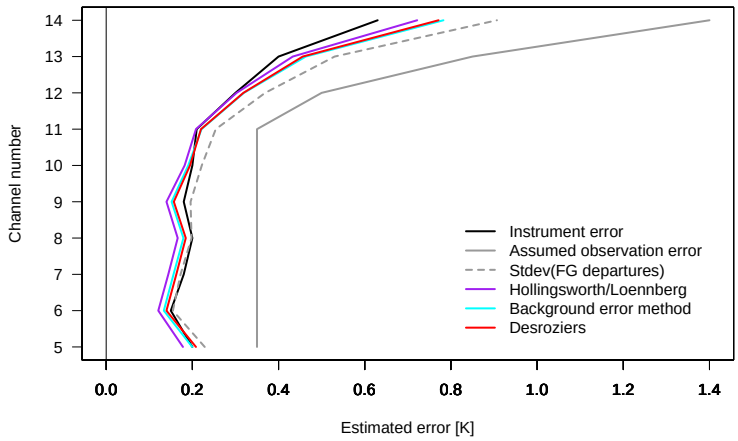

Figure 3: Estimates of observation errors for NOAA-18 AMSU-A channels used in the ECMWF system. The estimates are based on the measured in-flight instrument error (black), the observation error assumed in ECMWF's assimilation system (grey), the Hollingsworth/Lönnberg method (purple, calculated from the difference in FG-departure covariances at 0 km and 50 km separation), the background error method (cyan), and Desroziers' diagnostic (red). Also shown are the standard deviations of FG-departures (dashed grey).

estimates are fairly consistent and give relatively small spatial error correlations for AMSU-A for separations larger than the thinning scales currently used at ECMWF. For the current operational thinning scale of 125 km, the correlations are at or below 0.2 for all channels. Channels 5 and 6 have slightly higher correlations at short separation distances, but they are still relatively small (less than 0.3). Channels 5 and 6 have some sensitivity to the surface and to thick clouds and rain, and these aspects may lead to higher spatial error correlations, for instance, through the surface emission, undetected cloud or rain, or the quality control applied.

Estimates for the total observation errors are summarised in Fig. 3. Also shown are the standard deviations of FG-departures by channel which should provide an upper limit for the observation error, and the measured

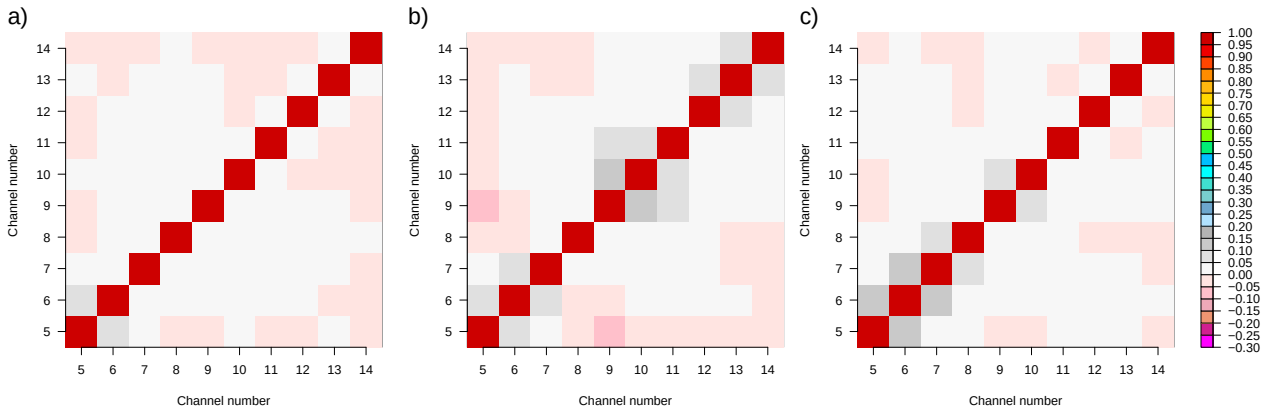

Figure 4: Estimates of inter-channel error correlations for NOAA-18 AMSU-A. a) Based on the Hollingsworth/Lönnberg method (calculated from the difference in FG-departure covariances at 0 km and 50 km separation). b) Based on the background error. c) Based on Desroziers' diagnostic. Note that the Desroziers diagnostic does not necessarily result in symmetric matrices; the matrices presented here have been made symmetric by using $\tilde{\mathbf{R}}' = \frac{1}{2}(\tilde{\mathbf{R}} + \tilde{\mathbf{R}}^T)$.

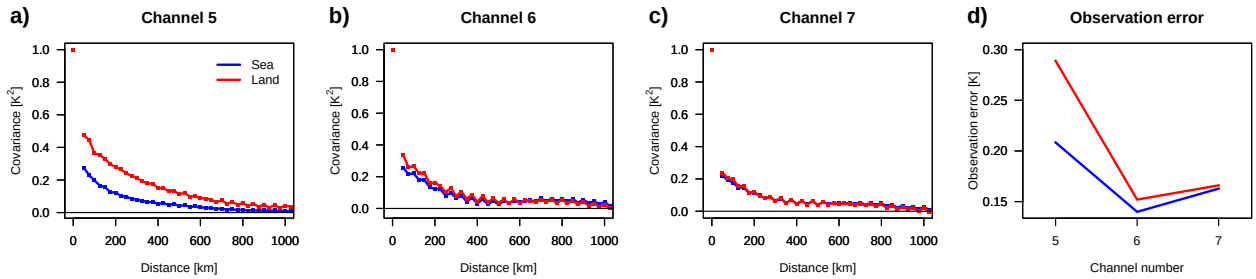

Figure 5: a) Comparisons of spatial observation error correlations as a function of separation distance over land (red) and sea (blue) from the Desroziers diagnostics for NOAA-18 AMSU-A channel 5. b) As a), but for channel 6. c) As a), but for channel 7. d) Estimates of the observation errors from the Desroziers diagnostic over land (red) and sea (blue).

mean instrument noise which should provide a lower limit of the observation error. The estimates for the three methods employed here are in good agreement, with values of less than 0.2 K for channels 5-10. For these channels, the estimates of the observation error are at or below the mean measured instrument noise. This is most likely due to sampling and quality control which will act to reduce the standard deviations of the FG-departures which are the basis of the observation error estimates. The finding nevertheless suggests that the radiative transfer error for these channels is relatively small, at least after applying the bias correction used in the ECMWF system. While intriguing, the latter result is consistent with the finding that spatial error correlations appear to be small, as radiative transfer errors are expected to be spatially correlated. The three estimates of observation error are much smaller than what is currently assumed as observation error in the ECMWF assimilation system, typically by about 40 %.

There is little evidence of inter-channel error correlations for AMSU-A (Fig. 4). The three methods employed here consistently give correlations of less than 0.2 between any channels. Desroziers' diagnostic gives the highest correlations between any channels, with around 0.13 between channels 5 and 6 and channels 6 and 7.

4.1.2 Land

The statistics presented so far were calculated for data over sea only; the same analysis has been repeated for data over land. Due to poor knowledge of the background errors and their correlations for skin temperature, the method of subtracting the scaled mapped background error gives poor results, so only the Desroziers diagnostic is available to estimate spatial error correlations. As expected, only channels 5 and 6 show appreciable differences in the observation error estimates, as other channels show little or no sensitivity to the surface characteristics. The Desroziers diagnostic suggests larger observation errors with stronger spatial error correlations, particularly for channel 5 (Fig. 5). The Hollingsworth/Lönnberg method also estimates larger observation errors (not shown), but the considerable size of the spatial error correlations suggested by the Desroziers method make the applicability of this method more questionable. Inter-channel error correlations between channels 5 and 6 are also increased slightly over land (by $\approx$0.05). The larger observation error estimates for the surface-sensitive channels over land are likely due to larger radiative transfer errors, as a result of a more difficult specification of the surface emission.

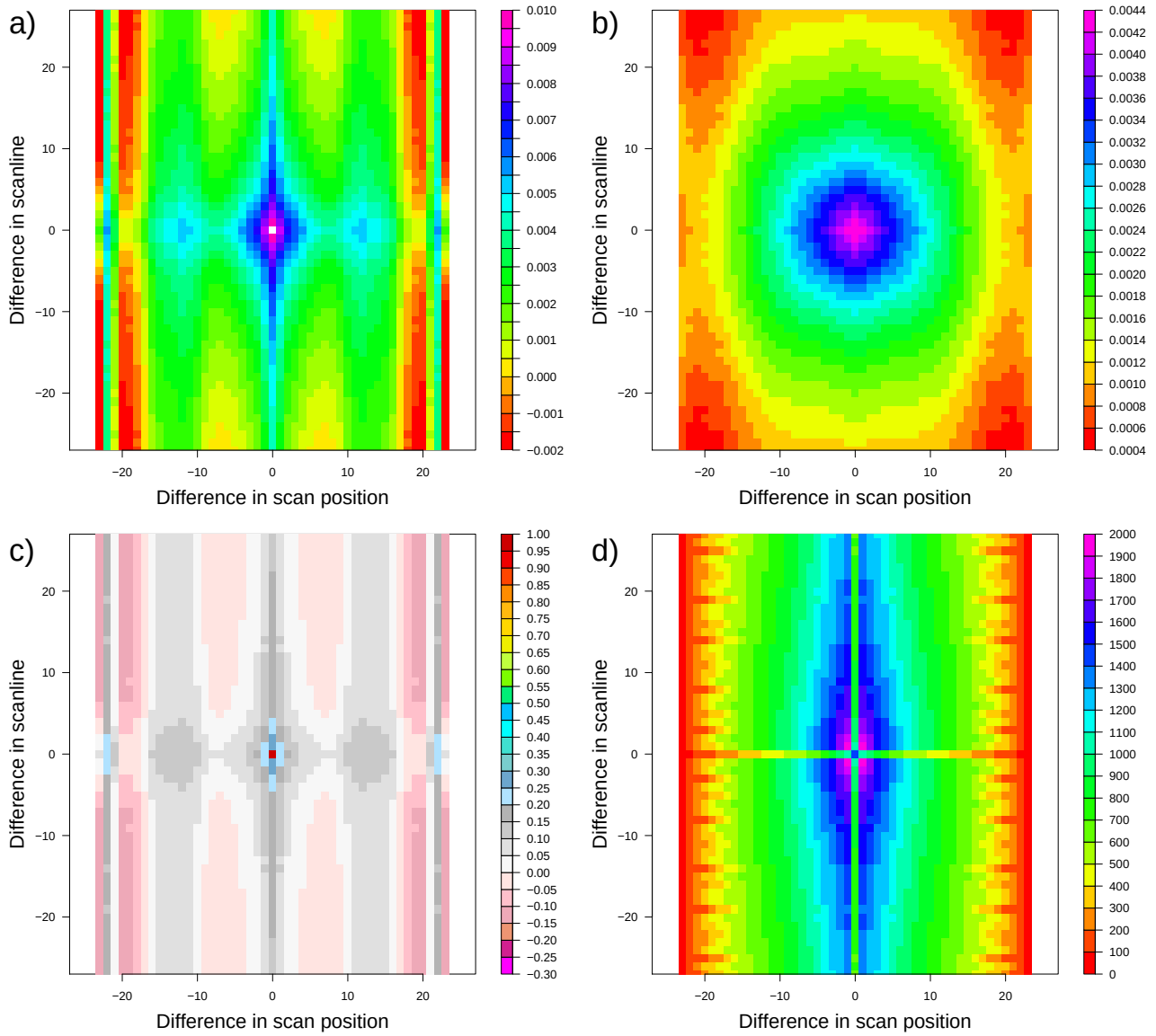

Figure 6: Diagnostics for NOAA-18 AMSU-A channel 6 over sea. a) FG-departure covariance statistics [K^2] as a function of scan position and scan line difference. The colour scale has been adjusted to emphasise values for non-zero differences; the FG-departure variance for zero separation is 0.024 K^2. b) Background error covariance estimates from the Desroziers diagnostic [K^2] as a function of scan position and scan line difference. c) As b), but for the observation error correlations. d) Number of observaton pairs used in thousands. Note that only one quadrant of each Figure has been calculated; the rest is derived from symmetry considerations.

4.1.3 Anisotropy

The error statistics have also been compiled as a function of the difference in scan position and scan line between the observation pairs, thus allowing for anisotropy. While for most channels FG-departure characteristics or observation error correlation estimates appear primarily isotropic, some channels show more complicated pattern. One example is channel 6 which shows some stripiness in the cross-track FG-departure covariances, in particular larger values for scan-position differences of 21 or 22 (Fig. 6 a). The pattern is satellite and channel-

specific; channel 6 on METOP-A, for instance, does not show the same pattern (not shown). Nevertheless, broadly similar characteristics have been found for channels 5-8 for some satellites. The reason for the features is unknown, but the finding that it is satellite-specific suggests an instrument-related scan characteristic that is not taken into account by the scan-bias correction. Consistent with this interpretation, the Desroziers diagnostics give a roughly isotropic estimate for the background error for channel 6 on NOAA-18, and attributes the stripes to correlated observation error (Fig. 6 b, c). As shown in our isotropic analysis, observation error correlations remain small, even with anisotropic features taken into account.

In summary, after bias correction, there is little evidence for considerable correlated error in the AMSU-A channels used at ECMWF, either spatially or between channels, except for small correlations for the lowest tropospheric sounding channels. Also, estimated observation errors are considerably smaller than what is currently assumed in the assimilation. While other aspects may need to be taken into account to set appropriate observation error covariances and thinning scales (e.g., influence of residual biases after bias control, analysis resolution), it appears that the current choice of observation errors and thinning scales used in the ECMWF system for AMSU-A is rather conservative.

4.2 MHS

We will now analyse data from the MHS instrument on METOP-A. MHS is a 5-channel cross-track scanning microwave radiometer, with the primary aim of sounding atmospheric water vapour around the 183 GHz water vapour band (e.g., Goodrum et al. 2009). It provides very dense sampling, with 16 km across-track and 17.6 km along-track at nadir. The quality control for MHS in the ECMWF system is as follows: Channels 3 and 4 are used over sea and low orography, whereas the use of channel 5 is restricted to data over sea only. No data is used over sea ice. Cloud or rain affected data are rejected when FG departures for channel 2 exceed 5 K. The outermost 9 scan positions on either side are also not considered for assimilation (out of 90 scan positions).

4.2.1 General results

Figure 7 shows covariances for FG-departures as a function of separation distance, compared to the estimates for the background error covariances from the Desroziers diagnostic and the background error assumed in the assimilation. The behaviour of the FG-departure covariances is quite different from that observed for AMSU-A: the covariances are much sharper with separation distance, reflecting the smaller correlation scales in the FG-errors for humidity. Also, there is no clear separation between the FG-departure covariance at zero separation

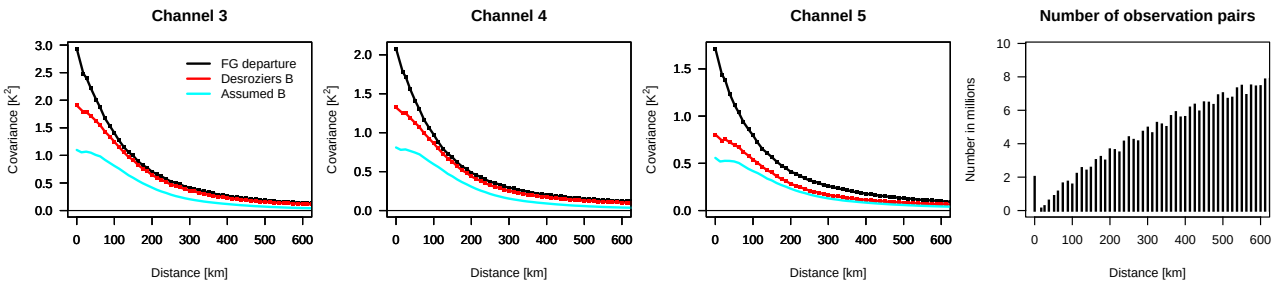

Figure 7: As Fig. 1, but for MHS on METOP-A with a binning interval of 12.5 km. Note also the smaller range of separation distances shown compared to AMSU-A.

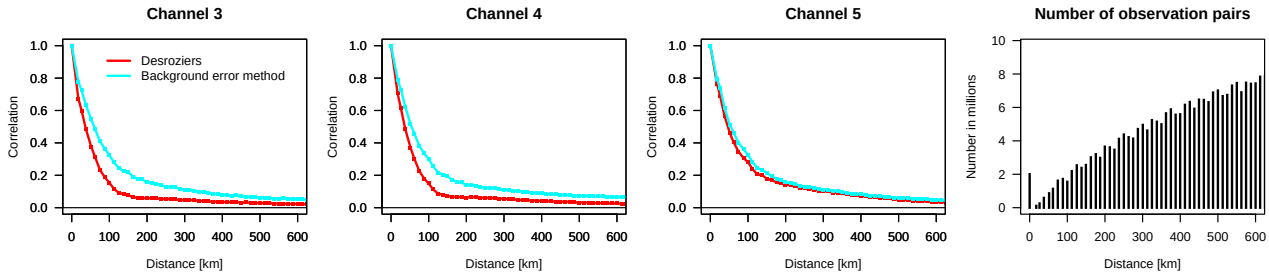

Figure 8: As Fig. 2, but for MHS on METOP-A. Estimates for the observation error correlations from subtracting values for the mapped background error covariances from the FG-departure covariances are based on unscaled values. Note also the smaller range of separation distances shown compared to AMSU-A.

and that at non-zero separation. This reflects that the relative contribution from the instrument error to the FG-departures is much smaller than was the case for AMSU-A (instrument errors for MHS are around 0.5 K, compared to standard deviations at zero separation of 1.3-1.7 K). Both aspects make it difficult to clearly separate the FG-departure covariances into a spatially correlated part (which is expected to be primarily due to FG-errors) and a spatially uncorrelated part (which is observation error). To reflect this, the finer spatial binning of 12.5 km has been used for the calculation of the FG-departure covariances.

The mapped assumed background errors and Desroziers' diagnostic background error show relatively good agreement in terms of the length-scales of the shorter spatial background error correlations. The assumed background errors are considerably smaller than the covariances computed from FG-departures or Desroziers' diagnostic background error estimate. The findings suggests that the assumed background errors are underestimated, or that some of the observation error for these MHS channels is spatially correlated.

For short separations (<200 km), the estimates of spatial observation error correlations for MHS are significantly larger than those obtained for AMSU-A. Figure 9 shows the estimates for spatial error correlations

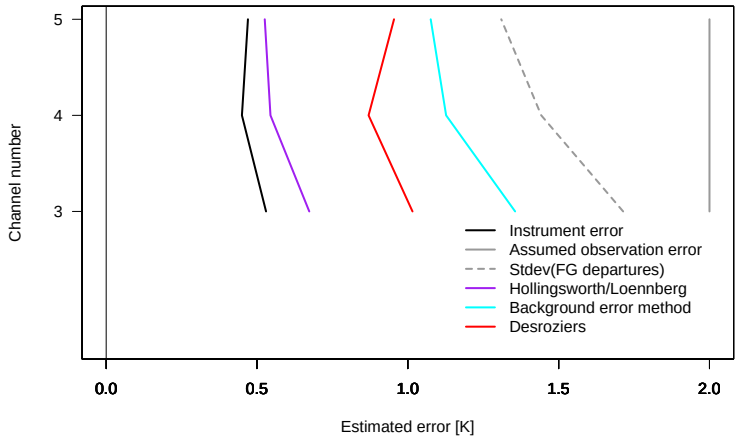

Figure 9: As Fig. 3, but for MHS on METOP-A. Estimates for the Hollingsworth/Lönnberg method are based on subtracting the FG-departure covariances from the 12.5 km bin (covering 6.25-18.75 km separations) from the FG-departure variances at zero separation. Estimates for the observation errors from subtracting values for the mapped assumed background error covariances from the FG-departure covariances are based on unscaled values.

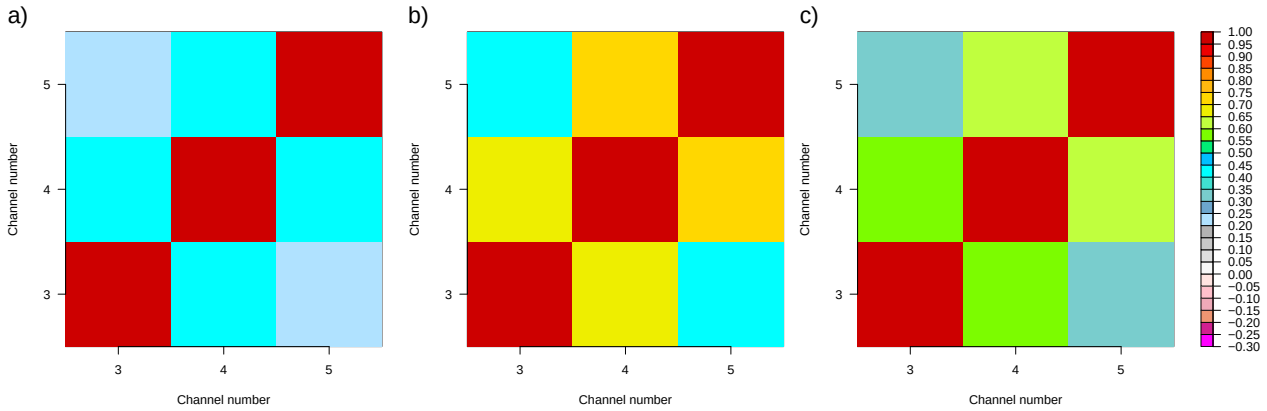

Figure 10: Estimates of inter-channel error correlations for METOP-A MHS. a) Based on the Hollingsworth/Lönnberg method (calculated from the difference in FG-departure covariances at 0 km and 12.5 km separation). b) Based on subtracting the unscaled mapped background error covariance from the FG-departure covariance. c) Based on Desroziers' diagnostic.

obtained from Desroziers' diagnostic and by subtracting the unscaled assumed background error covariance from the FG-departure covariances. Even though there are considerable differences between the two estimates, both indicate correlations close to or above 0.2 for some channels for separations of less than 140 km, the thinning scale currently used for MHS in the operational ECMWF system.

The estimates of spatial observation error correlations partly reflect aspects of representativeness. The analysis increments in the incremental assimilation system used here and the mapped background error estimates are calculated at a resolution of T255 (≈80 km), much coarser than the MHS FOV of 16 km (at nadir) and coarser than the model resolution of T799 (≈25 km). The mismatch in representativeness between the MHS FOV size and the resolution of the analysis increments will lead to errors of representativeness which are likely to be spatially correlated. Also, the FG for the FG-departures is used at full model resolution; any spatial FG-error correlations on finer scales than allowed by the coarser analysis increments will therefore be interpreted as spatially correlated observation error. Both aspects are much more prominent for observations sensitive to the humidity field with its small-scale variations and FG-errors than for temperature-sensitive observations.

Figure 9 gives estimates for the observation error for MHS. As expected, there is considerable variation between these estimates. The estimates from the Hollingsworth/Lönnberg method give the lowest observation errors, as they explicitly neglect any spatial correlations in the observation error. The values estimated with the Hollingsworth/Lönnberg method are therefore also closest to the instrument error. The other two methods provide estimates that are considerably larger than the instrument noise. This is partly a result of the representativeness issues discussed earlier, but may also be due to errors in the observation operator. The three methods again provide lower values for the observation error than what is currently assumed in the ECMWF system. Given that the representativeness issues discussed earlier should be reflected in the choice of observation errors, our estimates from the Hollingsworth/Lönnberg method are, however, not providing useful guidance for observation error specification for data assimilation systems for MHS.

Estimates for inter-channel error correlations are shown in Fig. 10. Again, there is some spread in the estimates for the error correlations, but all three methods employed here show significant inter-channel error correlations. Hollingsworth/Lönnberg gives the smalles values due to the reasons discussed earlier.

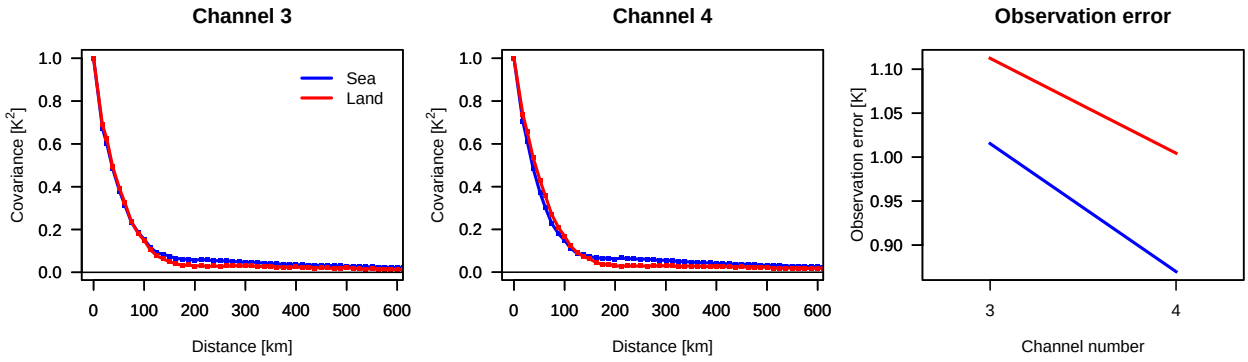

Figure 11: a) Comparisons of spatial observation error correlations as a function of separation distance over land (red) and sea (blue) from the Desroziers diagnostics for METOP-A MHS channel 3. b) As a), but for channel 4. d) Estimates of the observation errors from the Desroziers diagnostic over land (red) and sea (blue).

4.2.2 Land

Estimates for observation error covariances over land show only slight differences compared to the findings over sea. Only channels 3 and 4 are used over Land. The Desroziers diagnostic suggests slightly larger observation errors over land than over sea for these channels, but spatial or inter-channel error correlations are similar (e.g., Fig. 11).

In summary, our analysis gives indications for considerable inter-channel and some spatial observation error correlations for the three MHS channels used in the ECMWF system over land or sea. While the estimates for the observation errors are lower than what is currently used in the assimilation, some error inflation appears justified to counteract the effect of neglecting observation error correlations in the system.

4.3 HIRS

Next, we present results for the HIRS-4 instrument on METOP-A. HIRS is a 20-channel radiometer, with channels in the infrared and visible part of the spectrum (e.g., Goodrum et al. 2009). Sampling is 26 km across scan and 42.2 km along scan at nadir. The quality control applied to HIRS data in the ECMWF system is as follows: Channels 4-7, 11, 14, and 15 are assimilated over sea, whereas channel 12 is used over sea and land areas with low orography. Cloud screening is based on checks of the FG-departures and inter-channel gradients to identify clear channels (Krzeminski et al., 2009). The three outermost scan positions on either side in each scan are excluded (out of 56). The standard model used in the variational bias correction for HIRS is modified for channels 14 and 15 to include a predictor that is zero during night-time and the cosine of the solar zenith angle during daytime (Bormann et al. 2008).

4.3.1 General results

Spatial FG-departure covariances for HIRS are shown in Fig. 12. Channels 4, 5, and 15 show a clear separation into spatially correlated and spatially uncorrelated part. However, for channels 4 and 5 the FG-departure covariances for the 25 km separation bin (the bin with the shortest separations) are already considerably larger

than the 50 km bin, possibly due to very small-scale correlations for the observation error. For the other temperature channels (5, 6, 7, and 14) and the water vapour channels (11 and 12) the separation between spatially correlated and spatially uncorrelated part in the FG-departure covariances is much less clear: the covariances increase rather smoothly with decreasing separation distance. This makes the application of the Hollingsworth/Lönnberg method questionable, especially in the case of the water vapour channels which suffer from the same issues as outlined in the case of MHS. The covariances of the mapped assumed background errors show a similar behaviour compared to the FG-departure covariances as found for AMSU-A and MHS: for the lower temperature-channels, assumed background errors appear slightly too large, similar to what was seen for the lower-peaking AMSU-A channels, and for the water vapour channels, the mapped assumed background errors are at or below the FG-departure covariances.

Estimates for spatial observation error correlations are small for the long-wave temperature sounding channels, except for very short separation distances of less than 125 km, where they can exceed 0.2. For channel 7, the background error method gives slightly negative correlations around 200 km separation - most likely an artifact of insufficient scaling or poor representation of the spatial characteristics of skin temperature errors in our mapped background errors. Otherwise, estimates for spatial observation error correlations are similar for the two methods for the long-wave channels. For the short-wave temperature channels 14 and 15, there is some disagreement between the Desroziers diagnostic and the result from the background error method for the spatial observation error correlation. The Desroziers diagnostic gives broad correlations for both channels, reaching

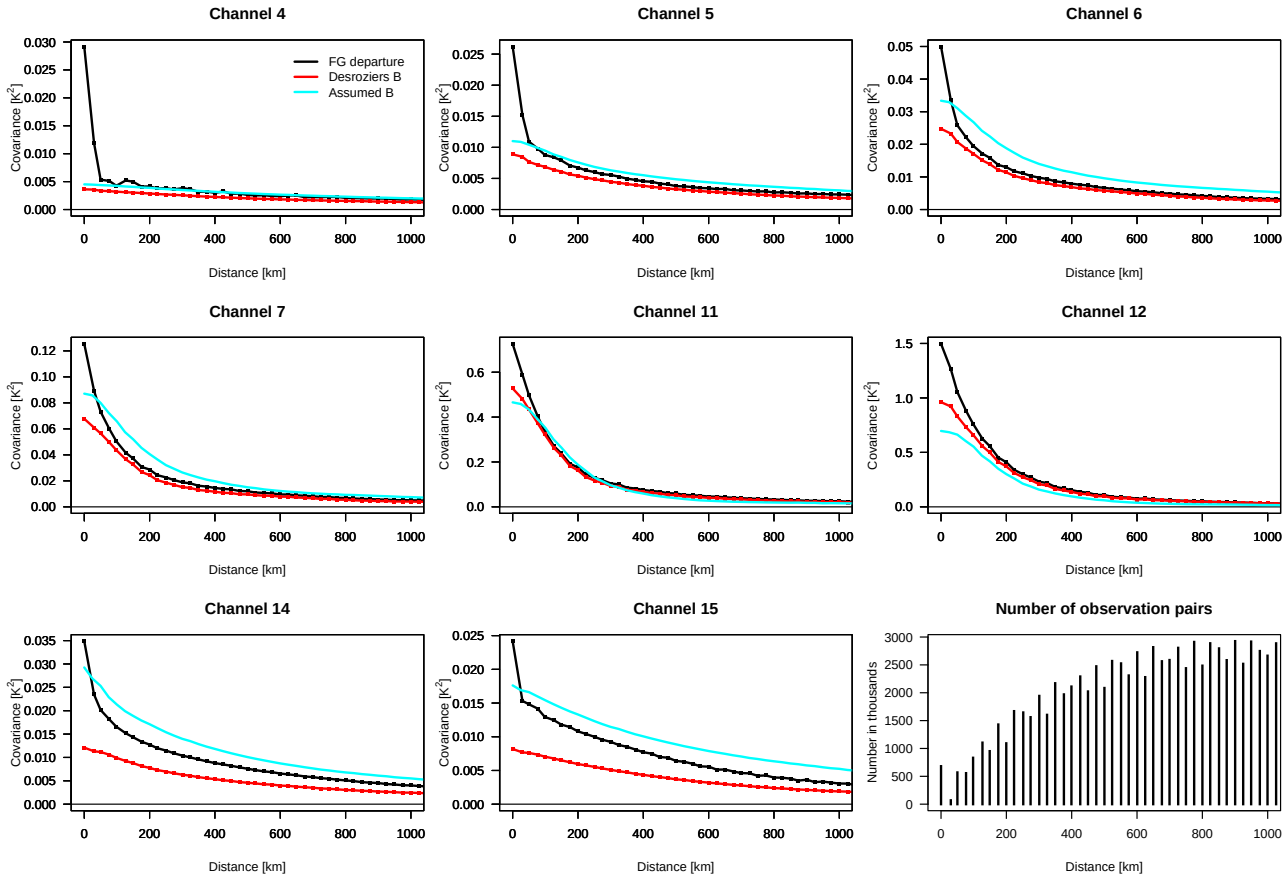

Figure 12: As Fig. 1, but for HIRS-4 on METOP-A.

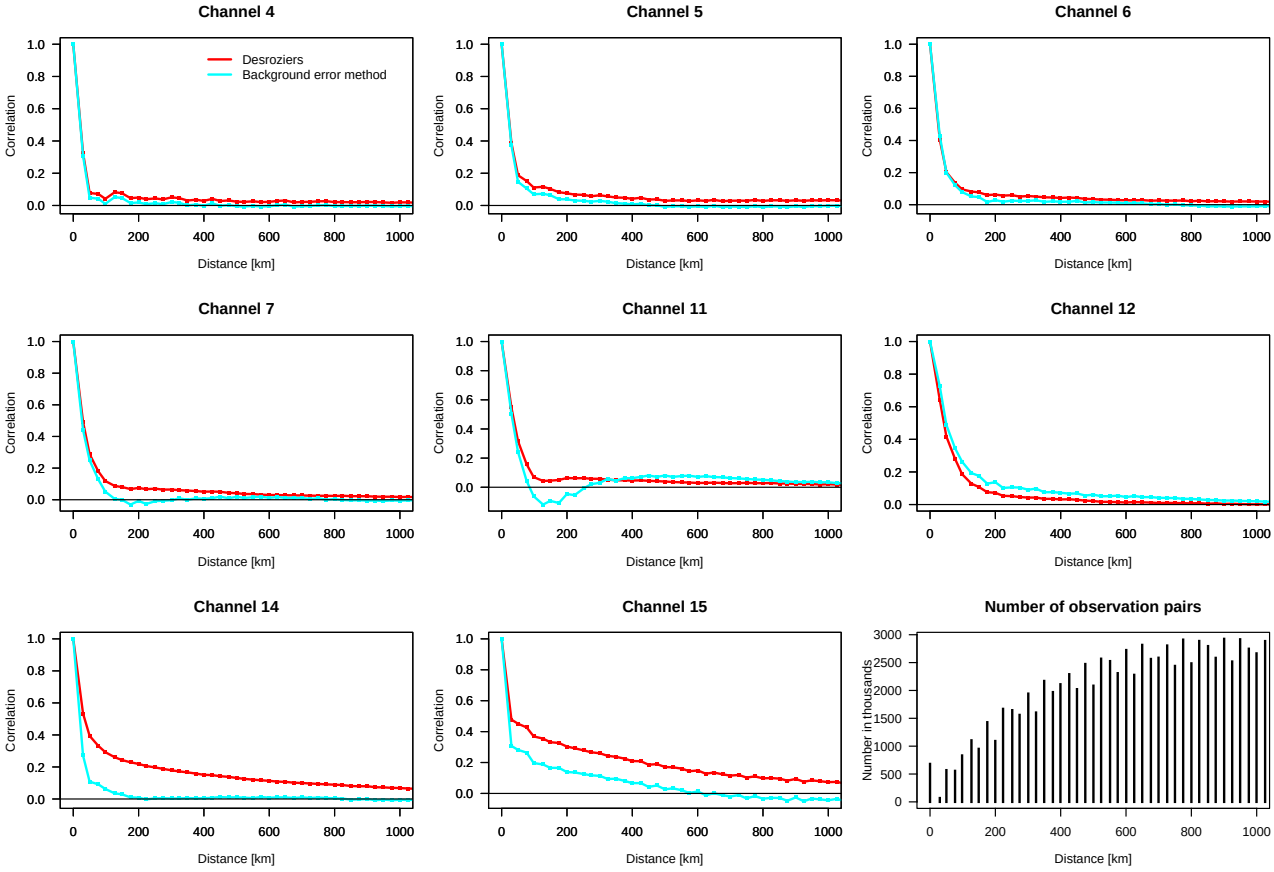

Figure 13: As Fig. 2, but for HIRS-4 on METOP-A.

0.2 at around 300 and 400 km, respectively. For channel 14, the background error method instead gives much smaller estimates. For channel 15, the background error method also indicates sizeable error correlations, albeit smaller than suggested by Desroziers. For this channel, the estimated error correlations for the background error subtraction method do not appear to converge to zero with increasing separations. This is likely due to insufficient scaling of the assumed background error, as the scaling is calculated with the assumption that observation error correlations are small for separation distances larger than 200 km. A smaller scaling factor would give more appropriate convergence to zero, leading to larger estimates of observation error correlation, in better agreement with Desroziers' diagnostic. It appears that the short-wave channels are more prone to spatially correlated errors, possibly due to poorer spectroscopy or due to contributions of other atmospheric gases that are held constant in our radiative transfer calculations (e.g., CO). For the water-vapour channels (11 and 12), the Desroziers diagnostic gives similar spatial error correlations as found for MHS, with considerable error correlations for short distances. For channel 11, the background error method gives again some artifacts, either due to insufficient scaling of the mapped background error characteristics or due to a misrepresentation of spatial scales in the mapped assumed background error.

Estimates for the size of the observation errors for HIRS-4 show reasonable agreement between the four methods used (Fig.14). For channels with the clearest separation of FG-departure covariances into spatially correlated and spatially uncorrelated part (4, 5, 15), the estimates are close to or even below the instrument noise. Again, values below the instrument noise are likely a result of sampling and quality control. The finding

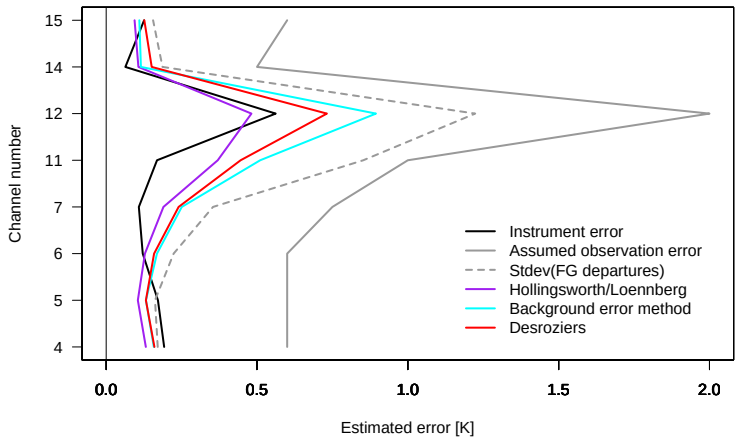

Figure 14: As Fig. 3, but for HIRS-4 on METOP-A. Estimates for the Hollingsworth/Lönnberg method are based on subtracting the FG-departure covariances for the 25 km separation bin from the FG-departure variances at zero separation. Estimates for the instrument noise have been converted to brightness temperature errors using the channel-specific mean observed temperature.

that the estimates are close to the instrument noise suggests that the radiative transfer error is small after bias correction. For channels more sensitive to the surface or the water vapour channels, the estimates for the observation error are larger than the instrument noise, most likely due to contributions from radiative transfer or representivity error. The exception is the estimate from the Hollingsworth/Lönnberg method for channel 12. Here, the estimate is below the instrument noise; however, the estimates for the water vapour channels from the Hollingsworth/Lönnberg method are considered less reliable due to the problems outlined for MHS. All estimates for observation errors are significantly smaller than the observation errors currently assumed, especially for temperature-sounding channels where the estimates are about a quarter of the currently assigned error.

The three methods employed consistently suggest sizeable inter-channel error correlations for HIRS-4 (Fig. 14). Particularly the lowest-peaking temperature channels (5, 6, and 7; 7 and 14) and the short-wave channels (14, 15) show correlations of 0.6 or higher for at least two methods. Cloud contamination, cloud screening, or errors in the surface emissivity are likely to contribute to this. The water vapour channels also show some inter-channel error correlations, but only of about 0.3-0.5.

4.3.2 Anisotropy

The Desroziers diagnostic has also been used to investigate error aspects as a function of difference in scan position and scan line, in order to check for anisotropic characteristics. Again, most channels show primarily isotropic features. However, channels 14 and 15 show additional structures. These are already aparent in FG-departure covariance statistics which show a clear striping, alternating between slightly higher and slightly lower values with the difference in scan position (e.g., Fig. 16 a). In addition, channel 15 exhibits higher FG-departure covarariances between scan positions located towards the edges of the swath. NOAA-17 HIRS data does not show the striping features to the same extent, but also shows higher FG-departure covariances between scan positions located towards the edges of the swath for observation pairs with small scanline differences (not shown). The Desroziers diagnostic attributes the additional structure primarily to correlated observation errors, although it also shows some anisotropic behaviour for the estimates of the background error (Fig. 16 b, c; note that the cross-track sampling for HIRS is finer than the along-track sampling, so the x- and y-axis scales correspond to different spatial scales). The latter possibly reflects that the weighting function for scan positions

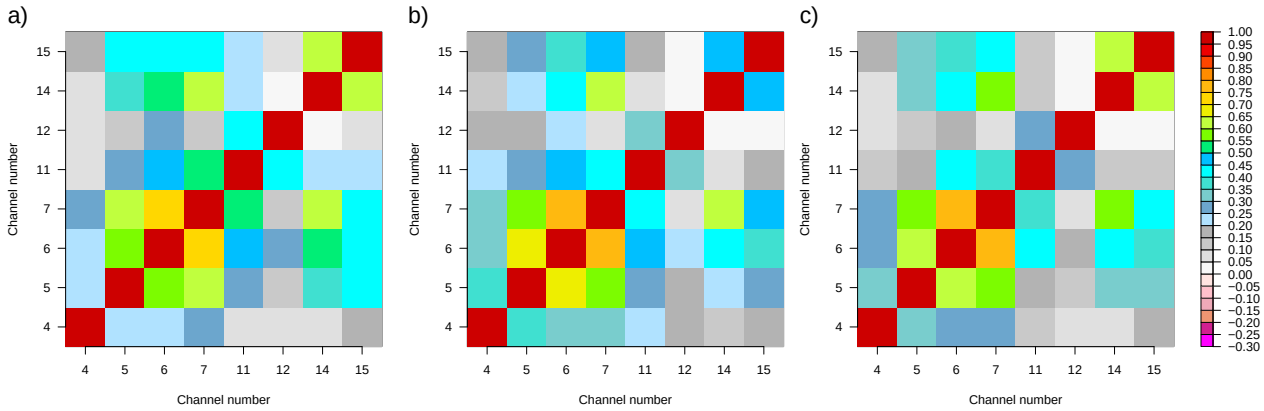

Figure 15: As Fig. 4, but for estimates of inter-channel error correlations for METOP-A HIRS-4. Estimates for the Hollingsworth/Lönnberg method are based on subtracting the FG-departure covariances for the 25 km separation bin from the FG-departure variances at zero separation.

located towards the edges of the swath will be shifted in the vertical due to the higher viewing angles. The reason for the pattern in the observation error correlations are unknown, but the characteristics suggest that they originate from the instrument design or the integration of the instrument on the satellite.

In summary, our analysis gives indications for considerable inter-channel error correlations and some spatial error correlations for the HIRS instrument. The use of somewhat inflated observation errors in the assimilation appears therefore justified to counteract neglecting these error correlations.

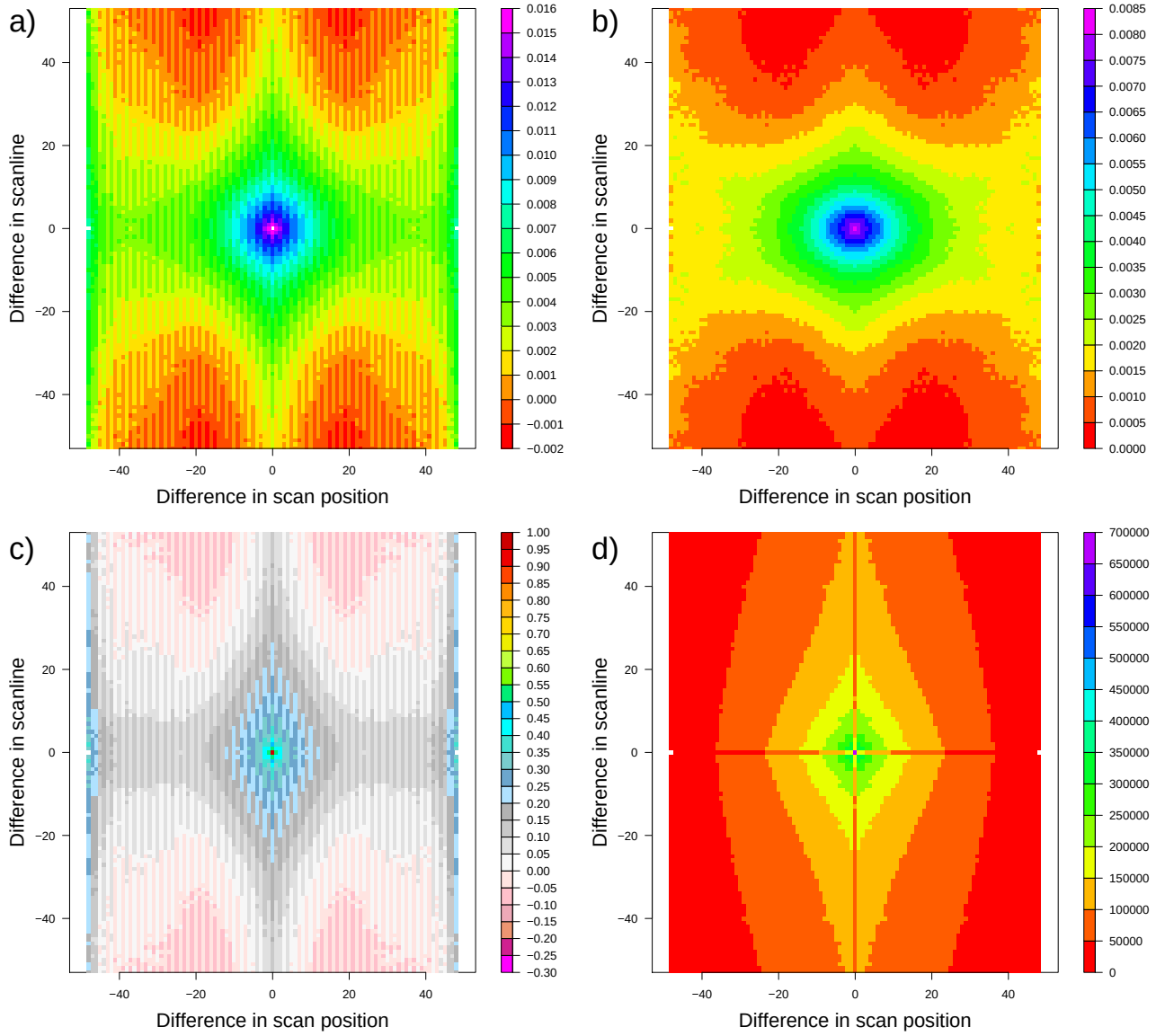

Figure 16: Diagnostics for METOP-A HIRS channel 15 over sea. a) FG-departure covariance statistics [K^2] as a function of scan position and scan line difference. The colour scale has been adjusted to emphasise values for non-zero differences; the FG-departure variance for zero separation is 0.024 K^2. b) Background error covariance estimates from the Desroziers diagnostic [K^2] as a function of scan position and scan line difference. c) As b), but for the observation error correlations. d) Number of observaton pairs used. Note that only one quadrant of each Figure has been calculated; the rest is derived from symmetry considerations. Also, the Figures show only entries for which more than 5000 observation pairs were available.

4.4 AIRS and IASI

We will now discuss the results for the advanced infrared sounders, AIRS on Aqua and IASI on METOP-A. AIRS is an infrared radiometer on Aqua with 2378 channels, covering the infrared part of the spectrum in three bands, 650.0 - 1136.6 cm^{-1}, 1217.0 - 1613.9 cm^{-1} and 2181.5 - 2665.2 cm^{-1} (Aumann et al. 2003). AIRS is flown together with an AMSU-A, and 3×3 AIRS FOVs are sampled per AMSU-A FOV. At ECMWF, only the warmest FOV within an AMSU-A FOV is considered for assimilation, as it is expected to be clearest. The outermost 9 scan positions on either side of the scan are also excluded. IASI is an Interferometer with 8461 channels covering the spectral interval from 645 - 2760 cm^{-1} with a spectral sampling of 0.25 cm^{-1} (Chalon et al. 2001). IASI provides 2×2 FOVs within an AMSU-A FOV; only the first of these is considered for assimilation at ECMWF (Collard and McNally 2009). The scan positions corresponding to the outermost three AMSU-A scan positions on either side of the scan are also excluded. Up to 119 AIRS and 175 IASI channels are used in the assimilation configuration used in this study; most of these are in the long-wave CO_2 band (Fig. 17). Cloud screening for both instruments follows the scheme of McNally and Watts (2003) which aims to identify clear channels based on evaluating FG-departure signatures. The scheme is applied to temperature-sounding channels; for the water-vapour band, the cloud-screening is linked to the results from the temperature-sounding channels. No IASI radiances are used over land, whereas up to 48 AIRS channels not sensitive to the surface are assimilated over land. The standard model used in the variational bias correction is modified for AIRS channels 1921 to 1928 to include a predictor that is zero during night-time and the cosine of the solar zenith angle during daytime (Bormann et al. 2008). Also, no air-mass bias correction is used for window channels (325 - 914 for AIRS, 380 - 1180 for IASI). Further information on the initial assimilation of AIRS and IASI data can be found in McNally et al. (2006) and Collard and McNally (2009), respectively.

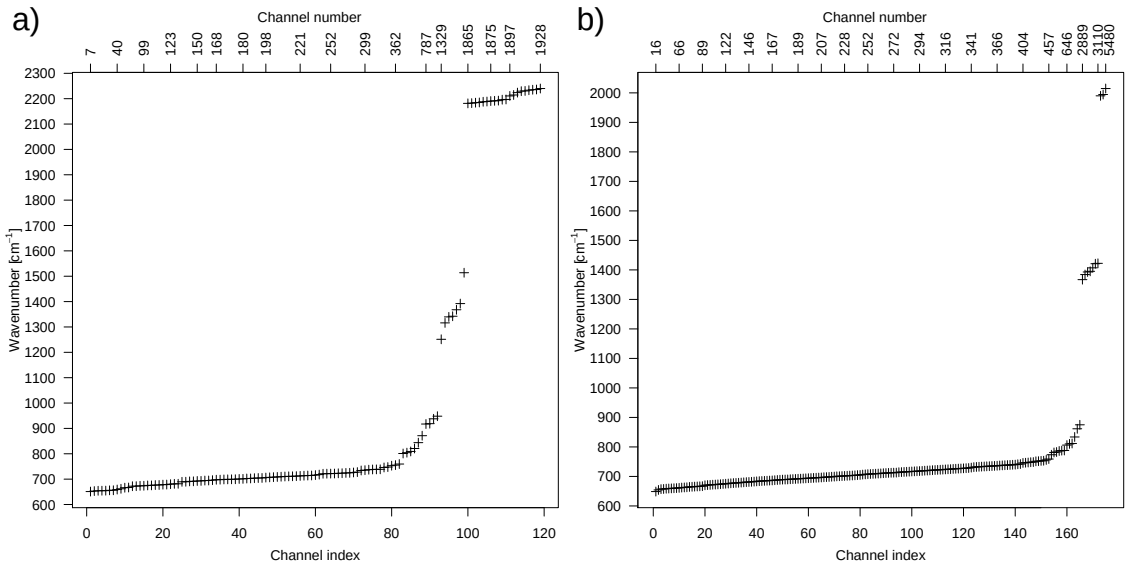

Figure 17: a) Wavenumbers [cm^{-1}] of the AIRS channels used in the ECMWF system as a function of channel index in the list of 119 channels. The top axis gives the values of selected AIRS channel numbers for further orientation. b) As a), but for the 175 used IASI channels.

Table 1: Groups of channels showing similar observation error characteristics for AIRS and IASI.

Group number	Description	AIRS channel numbers (wavenumbers [cm^{-1}])	IASI channel numbers (wavenumbers [cm^{-1}])
1	Long-wave CO_2, upper temperature-sounding	7 – 251 (651.05 – 721.54)	16 – 249 (648.75 – 707.00)
2	Long-wave CO_2, lower temperature sounding	252 – 355 (721.84 – 753.06)	252 – 445 (707.75 – 756.00)
3	Long-wave window channels	362 – 870 (755.36 – 948.18)	457 - 921 (759.00 – 875.00)
4	Water vapour channels	1329 – 1740 (1251.36 – 1513.83)	2889 - 3110; 5318, 5399, 5480 (1367.0 - 1422.25; 1990.0, 1994.5, and 2014.75)
5	Short-wave window channels	1865 – 1882 (2181.5 – 2197.0)	
6	Short-wave temperature sounding	1897 – 1928 (2210.85 – 2240.03)	

4.4.1 General results

The channels of each of the instruments can be broadly grouped into six groups that show different behaviour for the observation error covariance estimates. The groups are summarised in Table 1 and they will be further introduced below. The table also shows which channel range the groups are mostly covering; note that this separation should not be taken too strictly, as the groups overlap for some channels.

The first group of channels is characterised by spatial FG-departure covariances that show a very clear separation between a very small spatially correlated part and a much larger spatially uncorrelated part (see, for example, Figures 18 a-c). Just under half the channels used for each instrument fall into this group; they are the stratospheric to mid-tropospheric long-wave temperature-sounding channels. The estimated observation errors and their correlations show excellent agreement between the three methods. The size of the observation errors is close to the instrument noise which completely dominates the FG-departure variances (Figures 19 and 20). The channels show virtually no spatial error correlations right up to the smallest separation bin used (Figures 21 and 22), and small or no inter-channel error correlations (Figures 23 to 28). Similar to the case of AMSU-A, it appears that the radiative transfer error after bias correction is comparatively small. As in the case of similar AMSU-A channels, the spatial characteristics of the mapped assumed background errors are typically consistent with the FG-departure covariances or somewhat too large.

The second group of channels that share common characteristics in the observation error covariance estimates are lower-peaking temperature sounding channels in the long-wave band with weak sensitivity to the surface (surface transmissions of less than 0.2). What distinguishes this group is that the three methods consistently indicate the presence of some inter-channel error correlations between channels within this group (Figures 23 to 28). The size of these error correlations varies with channel pair, primarily in the range of 0.2 to 0.6, with the most surface-sensitive channels giving the highest inter-channel error correlations. The Hollingsworth/Lönnberg method and the background error method show remarkable agreement for the inter-channel error correlation estimates, whereas the Desroziers diagnostic tends to yield slightly lower values that

are still consistently non-zero.

The spatial FG-departure covariances for group two show a clear separation into a spatially uncorrelated and a spatially correlated contribution, with the latter being relatively larger than for the first group (see, for example, Fig. 18 d). The mapped assumed background error covariances appear generally too large when compared to the spatial FG-departure covariance statistics, and a scaling of down to around 0.3 is required for the lowest-peaking channels to make the two consistent. Nevertheless, Desroziers' diagnostic and the background error method give only weak spatial error correlations that stay below 0.2 even for the shortest separations and tail off rapidly (Figures 21 and 22). Consequently, the three methods employed here give very similar results for the size of the observation errors which are close to or slightly above the instrument noise (Figures 19 and 20).

The third group of channels are long-wave window channels with a surface transmission above 0.2. For these channels, FG-departure variances at zero separation are again dominated by a spatially uncorrelated component, as can be seen from the large difference between the values at zero separation and the first non-zero separation bin (see, for example, Fig. 18 e). The mapped assumed background errors are, however, generally considerably too large compared to the FG-departure covariances for non-zero separations, and the functional shape of the mapped background errors is such that no single scaling factor can be found to make the two curves consistent with each other. This is largely because the skin temperature background error has been modelled as spatially

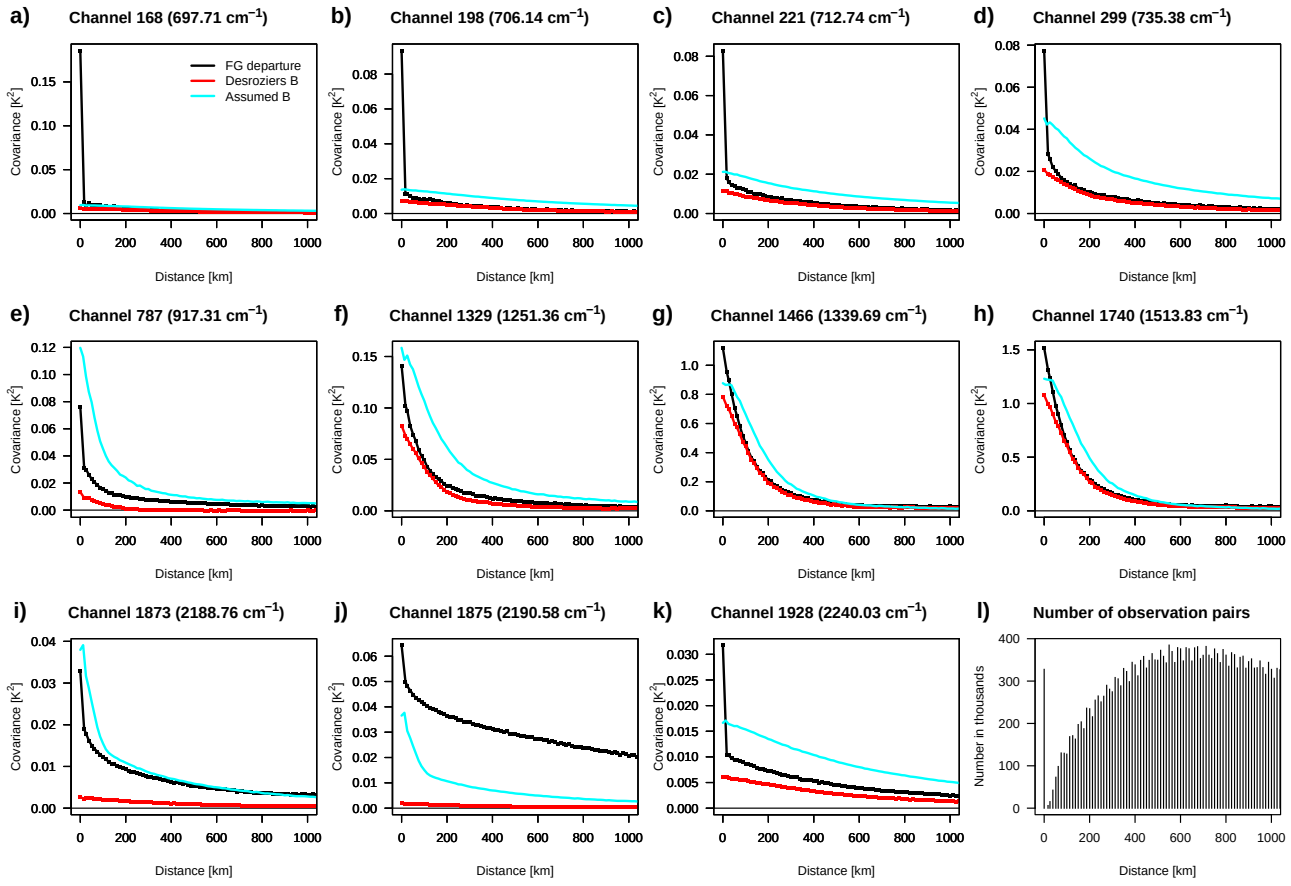

Figure 18: As Fig. 1, but for a selection of channels from AIRS on Aqua. The spatial binning interval is 12.5 km, and the wavenumbers for the selected channels are given in the title of each plot.

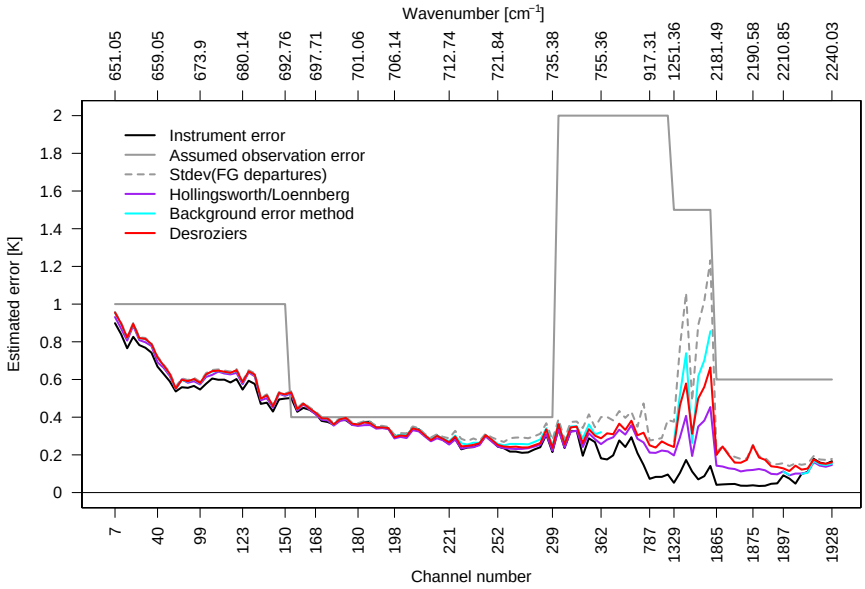

Figure 19: Estimates of observation errors for AIRS channels used in the ECMWF system. The estimates are based on the measured in-flight instrument error (black, converted to brightness temperature errors using the US Standard Atmosphere), the observation error assumed in ECMWF's assimilation system (grey), the Hollingsworth/Lönnberg method (purple, based on subtracting the FG-departure covariances for the 12.5 km separation bin from the FG-departure variances at zero separation), background error method (cyan), and Desroziers' diagnostic (red). For some channels, results from the background error method are not shown due to failure of the method (see text for further details). Also shown are the standard deviations of FG-departures (dashed grey). The lower x-axis gives the channel numbers for selected channels, whereas the upper x-axis shows wavenumbers for the corresponding channels.

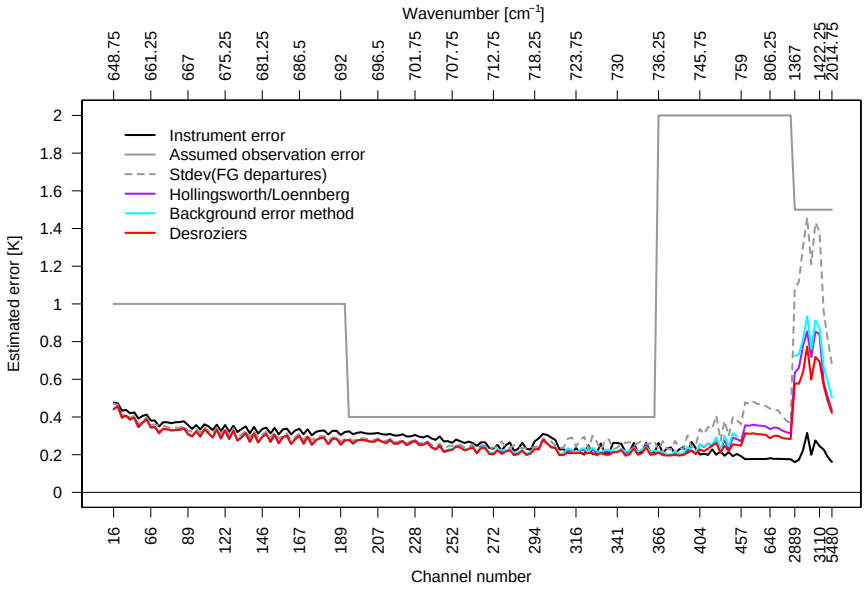

Figure 20: As Fig. 19, but for the IASI channels used in the ECMWF system. Estimates for the Hollingsworth/Lönnberg method are based on subtracting the FG-departure covariances for the 50 km separation bin from the FG-departure variances at zero separation)

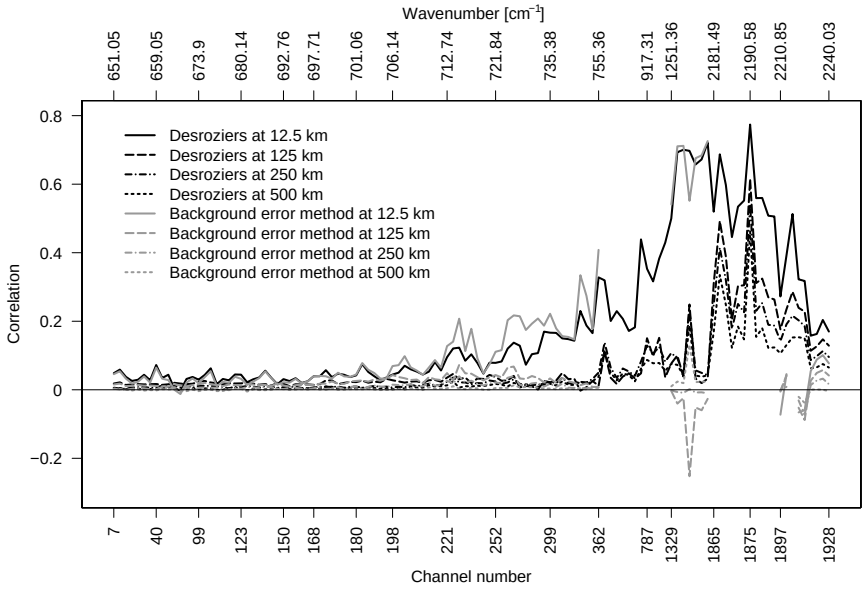

Figure 21: Estimates of spatial observation error correlations for selected spatial separation distance bins for the channels used in the ECMWF system. Black lines give estimates from Desroziers' diagnostic, grey lines from the background error method. Different line styles separate the selected separation distances as provided in the legend. For some channels, results from the background error method are not shown due to failure of the method (see text for further details).

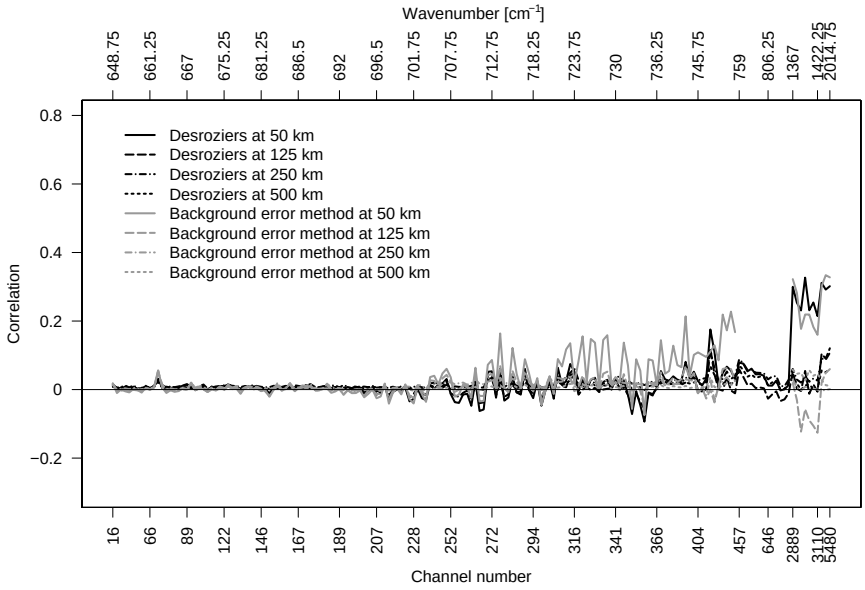

Figure 22: As Fig. 21, but for METOP-A IASI channels used in the ECMWF system. Note that in contrast to AIRS, the first populated separation bin for IASI is 50 km, compared to the 12.5 km bin for AIRS.

uncorrelated, whereas true background errors in skin-temperature are likely to be spatially correlated. The mapped background errors therefore show a too sharp decrease with separation distance for shortest separation distances. Given the limitations in modelling the spatial skin temperature error characteristics, the background error method is not applied for this group of channels. Desroziers' diagnostic therefore is the only method that provides estimates for spatial observation error correlations for these channels, and it indicates small spatial correlations in the range of 0.2-0.4 for the 12.5 km separation bin for AIRS, and rather small but broad and consistently non-zero correlations of around 0.05-0.1 beyond 500 km (Fig. 21). Estimates of the observation error are around 1.5-3 times the instrument noise, with reasonable agreement between the values from the Hollingsworth/Lönnberg method and the Desroziers diagnostics (Figures 19 and 20).

The most striking characteristic of the channels in group three are the rather strong inter-channel error correlations suggested by Hollingsworth/Lönnberg as well as Desroziers (Figures 23 to 28). For IASI, practially all channels show error correlations between each other, with values between 0.65 and 0.9. Again the Desroziers diagnostic tends towards smaller values in this range, but the block of correlated errors is very consistent with the estimate from Hollingsworth/Lönnberg. For AIRS, the block of inter-channel error correlations is less striking, but the group nevertheless exhibits error correlations between channel pairs within this group of 0.35-0.95. Channels from this group also show error correlations with channels from the second group to varying degree, typically in the range of 0.2-0.6.

The fourth group of channels are the water-vapour channels, with 7 AIRS channels and 10 IASI channels. These channels show many of the characteristics already noted for the HIRS or MHS water vapour channels. The spatial FG-departure covariances exhibit no clear separation of the variances at zero-separation into a spatially correlated and a spatially uncorrelated part - the transition is fairly smooth (see, for example, Fig. 18 f-h). The spatially uncorrelated part of the observation error is less dominant for the FG-departure variances than was the case for the temperature-sounding channels. This is again partly because instrument errors are much smaller compared to background errors for these channels. For IASI, instrument errors are around 0.2 K, and for AIRS they are even smaller, compared to background errors that are of the order of 1 K for mid- and upper-tropospheric water vapour channels (e.g., Fig. 18 g,h). Given the steep slope of the FG-departure covariances with separation distances, spatially uncorrelated observation error contributions of less than 0.4 K would be extremely difficult to detect with the Hollingsworth/Lönnberg method for these channels. As in the case of MHS, the Desroziers diagnostic as well as the background error method suggest some spatial observation error correlations for short separations, with values in excess of 0.6 for the 12.5 km separation bin for AIRS (Figures 21 and 22). They fall off fairly sharply to mostly less than 0.1 at 125 km or further. Representativeness issues are likely to be a contributing factor to these aparent spatial observation error correlations. Consequently, the estimates for the total observation error for the AIRS or IASI water vapour channels are considerably above the instrument noise, by a factor of 3-4 (Figures 19 and 20). As seen for MHS or HIRS, the three methods employed here indicate sizeable inter-channel error correlations for some of the water vapour channels, with many values between 0.6 and 0.9 (Figures 23 to 28).

The fifth group are short-wave window channels that are only used from the AIRS instrument. These channels show similar characteristics as the long-wave window channels in group three, in particular rather strong inter-channel error correlations. The Desroziers diagnostic and the Hollingsworth/Lönnberg method consistently estimate these to be frequently above 0.7 between most pairs of channels in this group, and around 0.25-0.6 between channels from this group and the long-wave window channels (Figures 23 and 25). The method of scaling the mapped assumed background errors again gives unrealistic results, due to poor modelling of the spatial characteristics of the skin temperature error. The results of this method are therefore not shown.

Group five shows additional characteristics to the ones in group two, suggesting a spatially correlated radiative transfer error. Whereas for the long-wave window channels the mapped assumed background error covariances at larger separation distances were consistently well above the FG-departure covariances, there are many

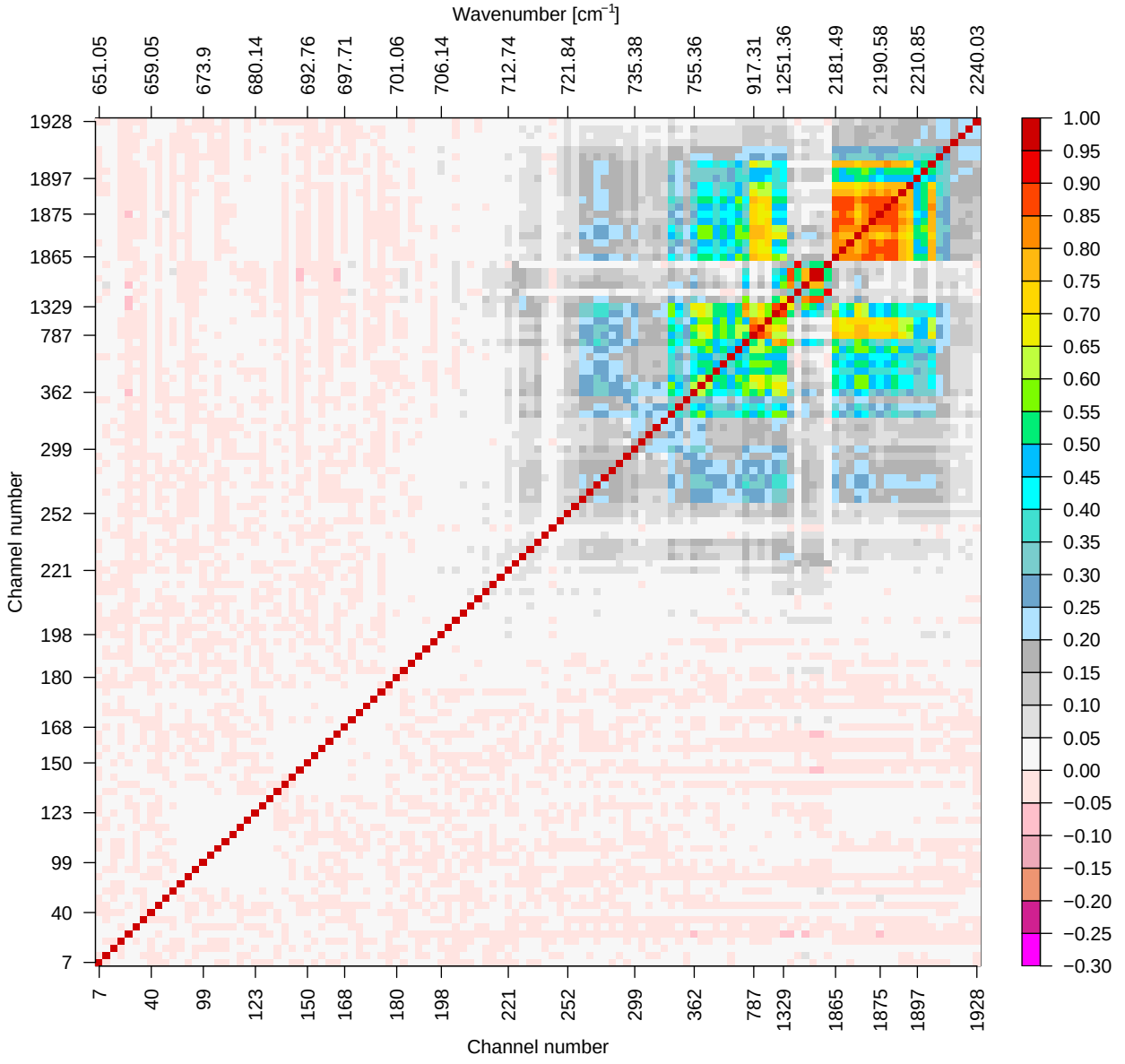

Figure 23: Estimates for inter-channel error correlations for the AIRS channels used in the ECMWF system, based on the Hollingsworth/Lönnberg method.

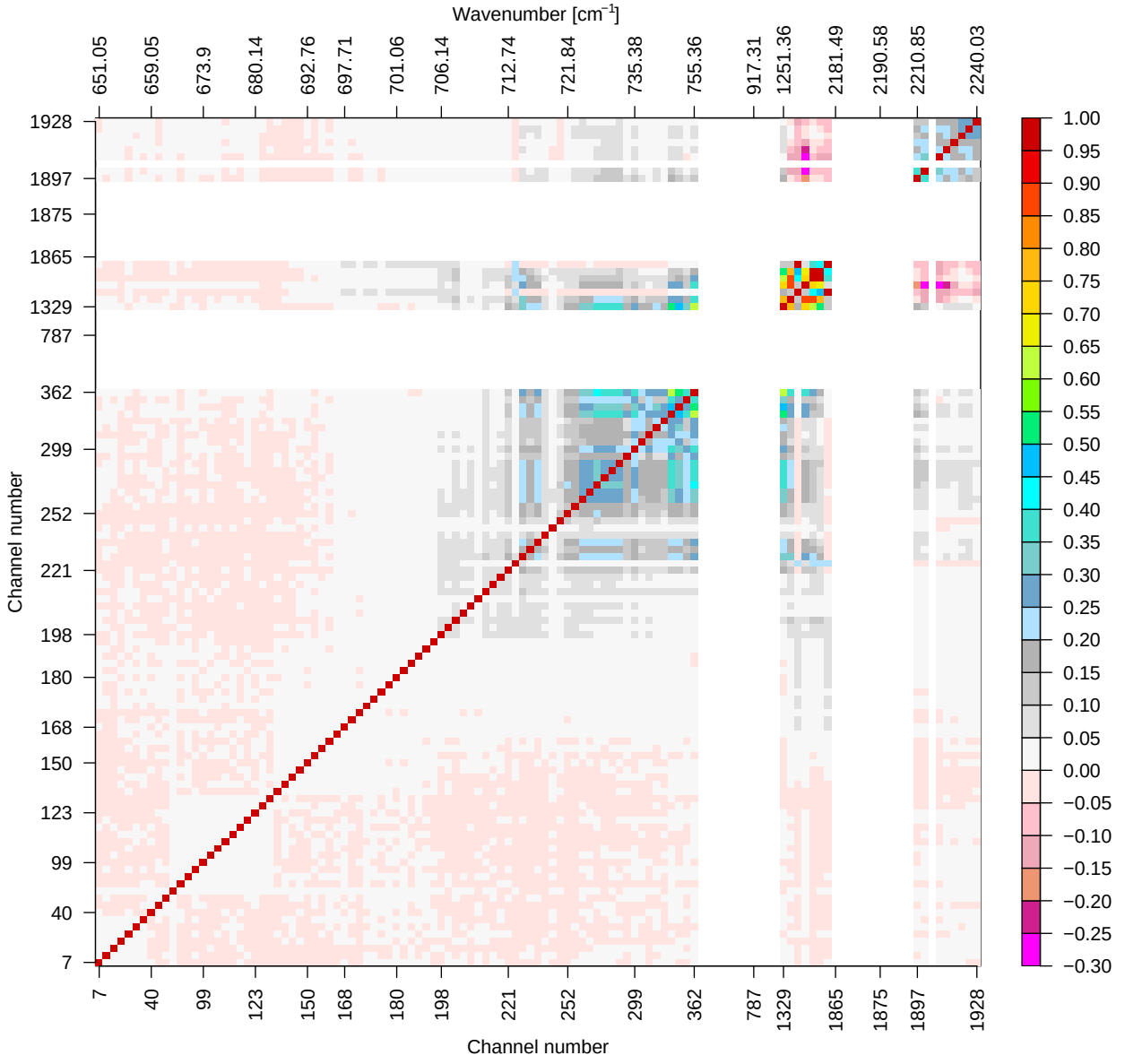

Figure 24: Estimates for inter-channel error correlations for the AIRS channels used in the ECMWF system, based on the background error method. Values for channels for which the method produced poor results appear white.

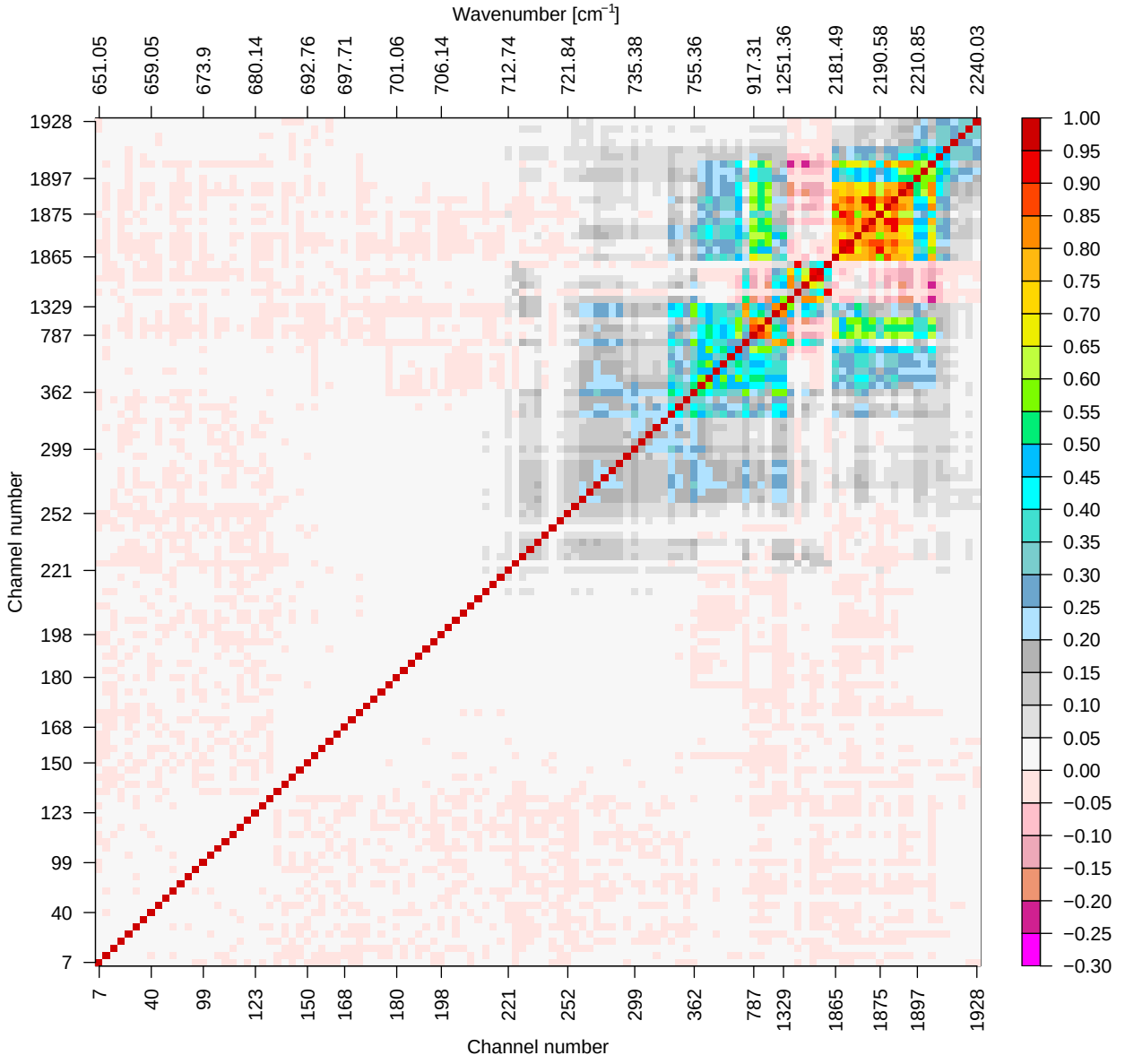

Figure 25: Estimates for inter-channel error correlations for the AIRS channels used in the ECMWF system, based on Desroziers' diagnostic.

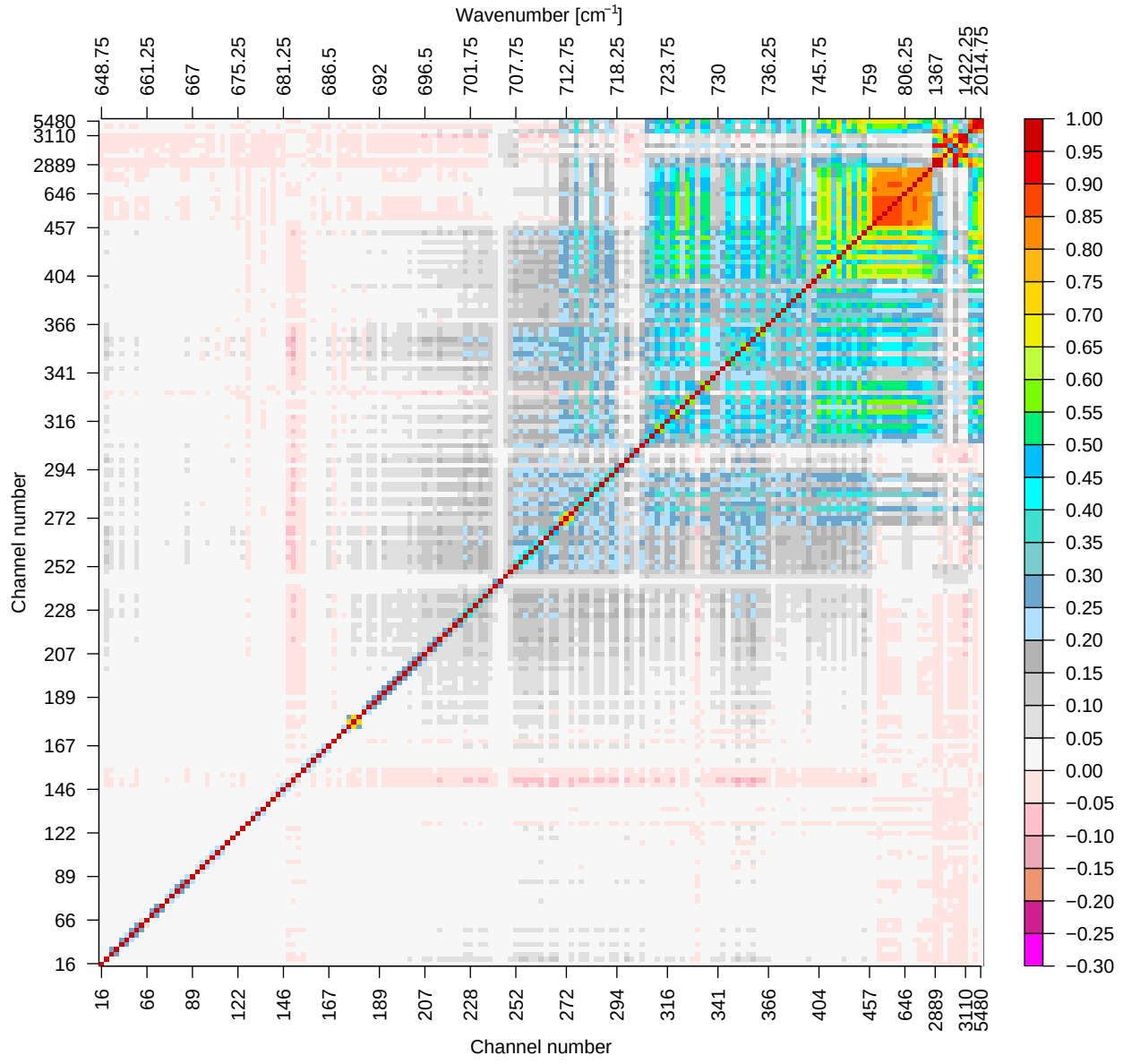

Figure 26: Estimates for inter-channel error correlations for the METOP-A IASI channels used in the ECMWF system, based on the Hollingsworth/Lönnberg method.

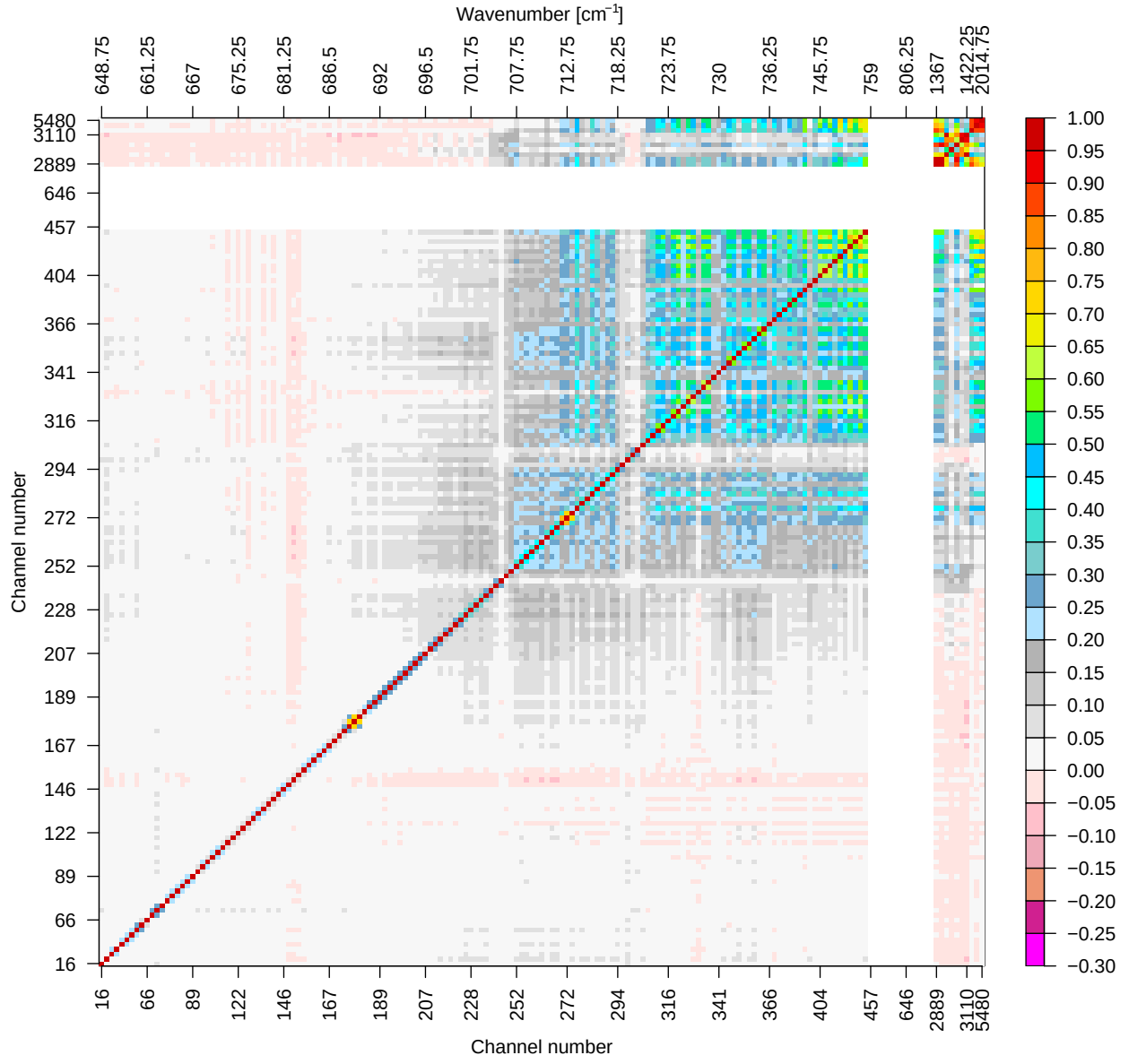

Figure 27: Estimates for inter-channel error correlations for the METOP-A IASI channels used in the ECMWF system, based on the background error method. Values for channels for which the method produced poor results appear white.

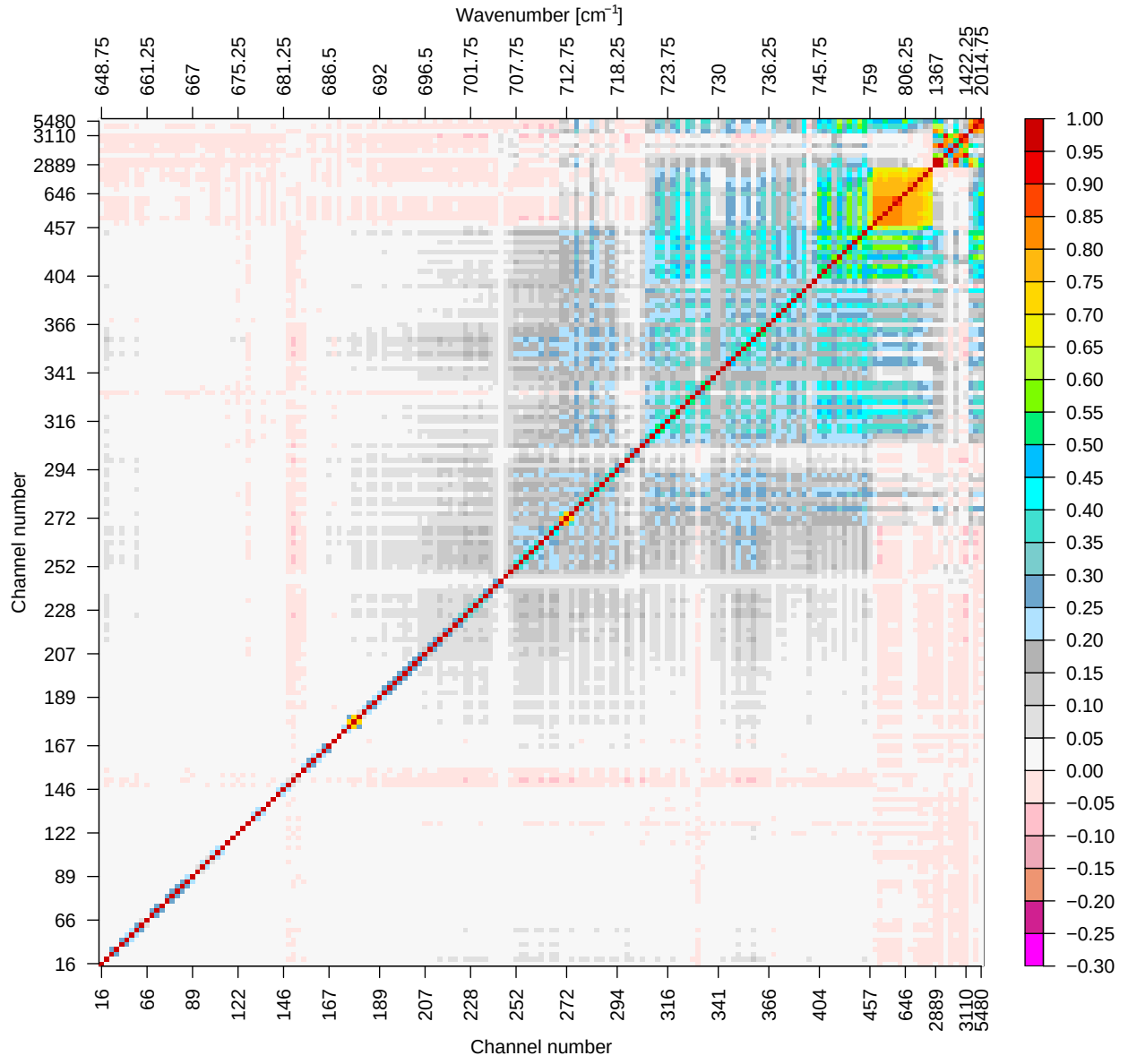

Figure 28: Estimates for inter-channel error correlations for the METOP-A IASI channels used in the ECMWF system, based on Desroziers' diagnostic.

channels in group five for which they are closer to or even well below the FG-departure covariances (see, for example, Fig. 18 i,j). This is particularly the case for channel 1875 (2190.6 cm^{-1}). The channel also stands out in the estimates for spatially correlated error from the Desroziers diagnostic (Fig. 21), where it exhibits very strong and very broad observation error correlations that are still above 0.3 at 1000 km separation. Further investigations reveal that the channel is very close to a CO line, and variations of CO are not taken into account in our radiative transfer model. As CO is not well-mixed, but rather shows strong hemispheric differences which would not project well onto our bias-correction model, this leads to a large and correlated radiative transfer error. Most channels in this group have some sensitivity to CO, contributing to larger and broader spatial error correlations as estimated from the Desroziers diagnostic. However, it should also be noted that the Desroziers diagnostic for the background error in radiance space is extremely small for channels in this group, and a skin temperature error well below 0.1 K would be required to achieve this, which appears unrealistic for the SST analysis used in the ECMWF system. The Desroziers method will be unable to successfully estimate observation or background errors when the scales respresented in both are too similar. The indicated spatial correlations in the observation error make it more similar to what is expected for background error correlations, so the results from the Desroziers method should also be taken with caution for this group.

The last group are lower-peaking short-wave temperature sounding channels, again only used for AIRS. These show largely similar characteristics as the lower-peaking long-wave temperature sounding channels in group two, with observation errors close to or slightly above the instrument noise (Fig. 19), and some inter-channel error correlations for the three estimation methods used here (Figures 23 to 25). Interestingly, error correlations between channels from this group and channels from group two are relatively small, suggesting a different origin for the error correlations. In contrast to the channels in group two, the channels in group six appear to exhibit broader spatial error correlations, in excess of 0.2 for the shortest separation bin and tailing off only fairly slowly with separation distance (Fig. 21). This is similar to the behaviour for the HIRS short-wave channels 14 and 15 located in the same spectral region (around 2210.0 and 2235.0 cm^{-1}, repectively, Fig. 13), and may be due to spectroscopy errors for this spectral region or other absorbers not allowed to vary in the radiative transfer calculations.

The estimated observation errors for AIRS and IASI are generally lower than the ones currently used in the ECMWF assimilation system (with the exception of channels 151 - 162 for AIRS; Figures 19 and 20). This is particularly the case for the surface-sensitive and window channels, for which the assumed observation errors are about five times the estimates found in this study. This reflects a cautious approach for these channels, justified due to the smaller atmospheric temperature signal in these channels in clear-sky cases and also due to the inter-channel error correlations found for these channels which are currently neglected in the ECMWF assimilation system. The step in the assumed observation error from 1.0 K for the stratospheric channels to 0.4 K for the tropospheric channels seems somewhat arbitrary. For most of the mid to upper tropospheric channels (151 - 299 for AIRS and 191 - 366 for IASI), the assumed observation errors are actually fairly close to the the observation error estimates obtained in this study; they are the closest encountered for any of the instruments investigated here.

4.4.2 IASI-specific results

In the case of IASI, another aspect evident from the estimates of inter-channel error correlations is worth mentioning. The three methods consistently estimate non-zero error correlations for the first off-diagonal element in the inter-channel error correlation matrix for many channels (Figures 26 to 28). This is due to the apodization used for IASI, which leads to non-zero error correlations for channels that are up to two channels apart and which are strongest for directly neighbouring channels. The effect of this is clearly visible in the statistics: two triplets of channels that are direct neighbours stand out with error correlations of 0.7-0.75, whereas channels

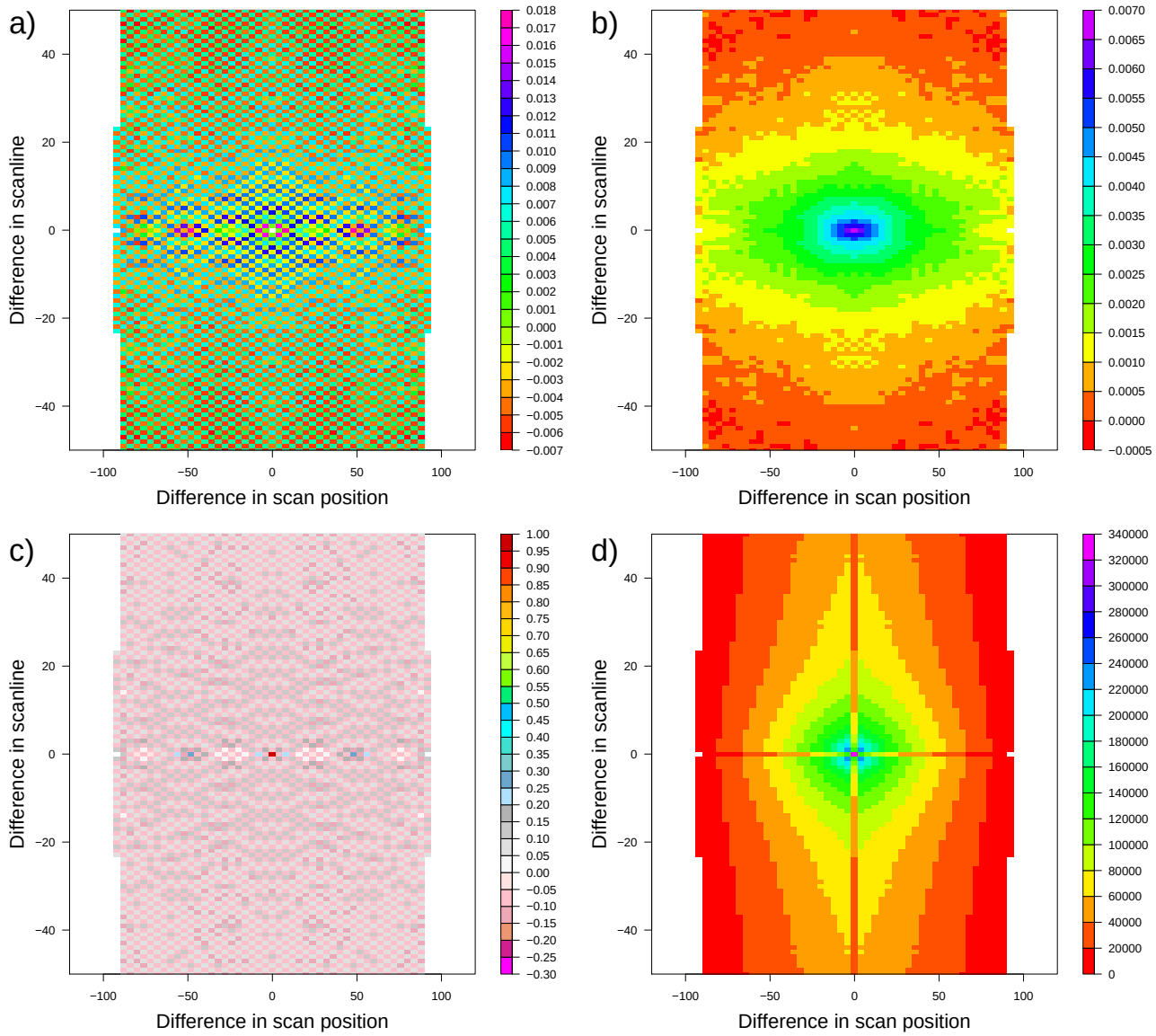

Figure 29: Diagnostics for METOP-A IASI channel 360 (734.75 cm^{-1}) over sea. a) FG-departure covariance statistics [K^2] as a function of scan position and scan line difference. The scan position used is the one provided in the disseminated data, with values from 0 to 119. The colour scale has been adjusted to emphasise values for non-zero differences; the FG-departure variance for zero separation is 0.064 K^2. b) Background error covariance estimates from the Desroziers diagnostic [K^2] as a function of scan position and scan line difference. c) As b), but for the observation error correlations. d) Number of observaton pairs used. Note that only one quadrant of each Figure has been calculated; the rest is derived from symmetry considerations. Also, the Figures show only entries for which more than 5000 observation pairs were available.

that are one channel apart show error correlations of around 0.25-0.35 in the absence of further error correlations due to other reasons. Neighbouring channels were originally excluded in the IASI channel selection for Numerical Weather Prediction (Collard, 2007), but the channels in question were later added for monitoring purposes.

Almost all IASI channels exhibit a peculiar pattern in the FG-departure covariances when analysed as a func-

tion of the difference in scan line and scan position. These covariances show a chessboard pattern of lower and higher FG-departure covariances as seen in Fig. 29 a for channel 360 which shows it the clearest. Note that always the same IASI FOV position within an AMSU-A FOV is used at ECMWF. Using the IASI scan position numbering from 0 - 119 within an AMSU-A scan line (as provided in the disseminated data), the FOVs currently selected at ECMWF are multiples of 4. Possible scan position differences for our analysis are therefore also multiples of four. The feature also shows up as wiggles in the isotropic analysis of FG-departure covariances at short separation distances, such as the ones in Fig. 18 (not shown). The magnitude of the feature is dependent on the channel, but practically all channels show at least a hint of this feature (Fig. 30). The Desroziers diagnostic attributes the feature to a pattern of alternating positive and negative observation error correlations (Fig. 29 c). The chessboard feature has also been observed in FG-departure covariances obtained at the Met.Office (Cameron 2009, pers. communication).

The pattern is very small compared to the instrument noise (as aparent from rather small estimated observation error correlations), and it is of no concern to the assimilation of the data. The feature appears to correlate with the direction of the movement of the corner-cube mirror of the IASI interferometer (Fiedler 2009, pers. communication). The current understanding is that this is the first evidence of the existence of pseudo-noise ("ghosts") caused by micro-vibrations of IASI's beam splitter (Blumstein 2009, pers. communication). Such effects are expected for instruments like IASI. The beam splitter is fixed on one side to the optical bench and displays a slight periodic variation in position with respect to the corner-cube motion. This leads to slight variations in the spectral characteristics which appear as pseudo-noise. Consistent with this explanation, investigations at the Met.Office found that the chessboard effect is almost zero for those IASI FOVs that project onto the bottom of the beam-splitter where the effect of the vibrations is smaller as this is where the beam splitter is attached to the

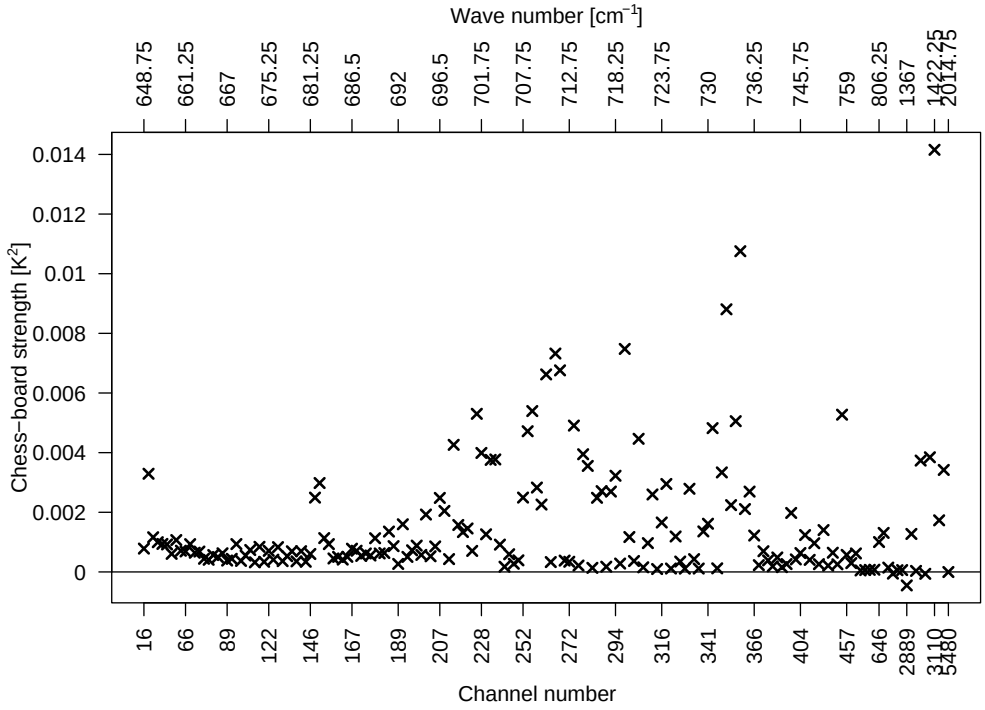

Figure 30: Strength of the chessboard pattern in the FG-departure covariances as a function of channel number [K^2]. The strength has been calculated as the mean difference between the two populations given by the chessboard pattern of high and low FG-departure covariances (excluding the values at zero separation).

optical bench. That is, selecting the 3rd or 4th IASI FOV within the AMSU-A FOV minimises the chessboard effect. It is remarkable that the monitoring against the FG can detect such small effects which so far have not been picked up in careful monitoring of the instrument's engineering data. Our investigations also confirm that the effect is as small as expected.

4.4.3 Comparison to results from Garand et al.

The estimates for observation errors and inter-channel error correlations for AIRS can be compared to those obtained by Garand et al. (2007). A stringent comparison is difficult due to different channel selections. Nevertheless, our results are consistent with Garand et al. (2007) for most channels of group one, both in terms of the size of observation errors and the lack of significant inter-channel error correlations. For lower-peaking temperature sounding or window channels in the longwave (groups two and three), Garand et al. (2007) also find significant inter-channel observation error correlations, but their estimates are larger than in the present study, also with larger observation errors. The situation is similar for the water vapour channels. The reasons for the differences are unclear, but may be due to differences in the approach to bias correction (variational with air-mass predictors vs static with observed brightness temperatures as predictors) or the cloud detection. Undetected cloud contamination may lead to larger observation errors which appear correlated between channels in the Garand et al. (2007) study, or too strict FG-departure based cloud detection may give overly optimistic observation errors in the present study. For the short-wave window channels, our estimates of observation errors are again lower than presented in Garand et al. (2007), but the finding of substantial inter-channel error correlations is consistent.

4.5 Findings for assumed background errors

While our main focus is the characterisation of observation error covariances for sounder radiances, our analysis also provides information on the assumed background error covariances. As already mentioned, the spatial correlation characteristics of the assumed background errors mapped to radiance space appear, on average, consistent with FG-departure covariances, at least for temperature-sounding channels. However, there were also indications that the magnitude of the background errors appears occasionally overestimated. To address this, the background error method produces channel-specific scaling factors which have been derived by matching spatial FG-departure covariances with assumed background errors mapped into radiance space. The Desroziers diagnostic (2) provides estimates of background error covariances mapped into radiance space directly. A channel-specific scaling factor can also be derived which matches the spatial background error covariance estimates from the Desroziers diagnostic with the assumed background errors mapped into radiance space.

Figure 31 shows an intercomparison of the scaling factors for the background errors for all temperature-sounding channels of the various instruments used in this study as a function of the peak of the weighting function. There is considerable consistency in broad features of these scaling factors between different channels and instruments. Some scatter is to be expected, as the peak of the weighting function is only a crude measure of the sensitivity of the channel in the vertical. Scaling factors are typically around 0.6-0.8 for the troposphere, indicating an inflation of the assumed background error in this area. In contrast, for most of the stratosphere, scaling factors are around 0.9-1.0, suggesting little or no inflation of the background errors. Not surprisingly, there is good consistency also between the scaling factors from the background error method and those obtained with the Desroziers diagnostic. The Desroziers diagnostic tends to produce smaller scaling factors, as the assumption on spatially correlated observation errors is more relaxed for this method, so less of the FG-departure covariances is attributed to background error.

The agreement for humidity scaling factors is less good between different instruments, even though the back-

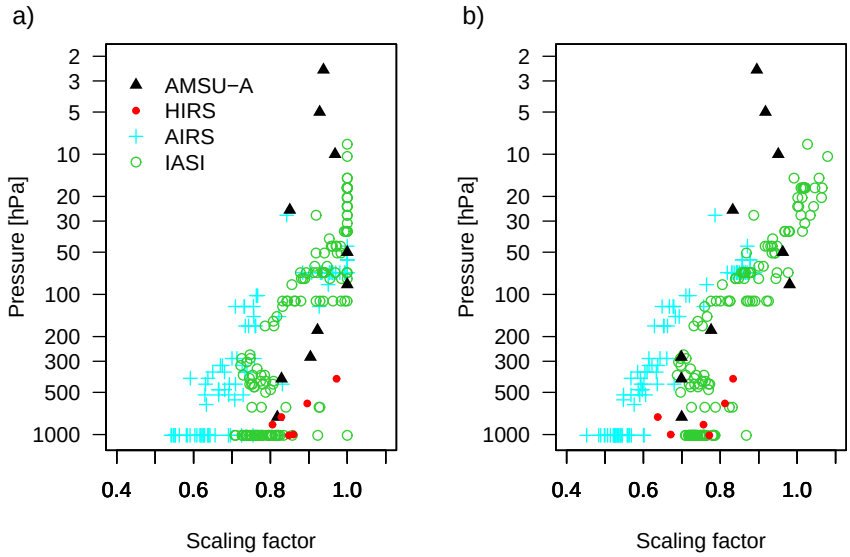

Figure 31: a) Scaling factors for the background errors for the temperature sounding channels used in this study, as derived in the background error method. The scaling factors are plotted as a function of the peak of the weighting function for the various channels. Different symbols and colour-coding indicate the four temperature-sounding instrument considered in this study, as given in the Figure legend. Note that the scaling factors in the background method are restricted to values less than or equal to one. b) As a), but for scaling factors for the background errors as derived from the Desroziers diagnostic.

ground error method and the Desroziers-derived scaling factors again agree fairly well. Scaling factors range from around 0.8 for the AIRS water vapour channels to 1.1-1.2 and 1.2-1.6 from the Desroziers diagnostic for the HIRS water vapour channels and MHS, respectively.

5 Conclusions

In the present study we have estimated observation errors and their spatial and inter-channel error correlations for clear-sky radiances from the main sounding instruments currently assimilated at ECMWF. The findings are:

- AMSU-A shows little spatial or inter-channel observation error correlations for all channels used in the assimilation. Estimates of the observation error are close to the instrument noise. The current use of thinning scales and observation errors appears very conservative for AMSU-A.
- Mid-tropospheric to stratospheric temperature sounding channels for AIRS and IASI also show little or no inter-channel or spatial observation error correlations, and estimates for the observation error are close to the instrument noise.
- The finding that observation errors for mid-tropospheric to stratospheric temperature sounding channels for the longwave infrared or the microwave instruments are comparable to the instrument noise suggests that the radiative transfer error is small after bias correction for these channels.

- Channels with stronger sensitivity to the surface show larger observation errors compared to the instrument noise, and some of this error is correlated spatially and between channels. This is particularly true for the infrared instruments (HIRS, AIRS, and IASI), but also, to a lesser extent, for AMSU-A. Residual cloud contamination may be a contributing factor to this. Infrared window channels can exhibit very high inter-channel error correlations of more than 0.7.

- Short-wave infrared temperature sounding channels appear more prone to spatial observation error correlations, probably a result of larger errors in the spectroscopy (e.g., due to more line mixing effects) or other contaminating gases (CO).

- Estimating observation errors for humidity sounding channels from FG or analysis departures is more difficult, primarily due to the combination of smaller-scale and larger errors in the FG for humidity. A considerable proportion of the observation error for humidity sounding channels appears correlated spatially for short separation distances, as well as between channels. Representativeness appears to be an important contributor in this respect. Observation error estimates for humidity channels are generally considerably larger than those provided by the instrument noise.

- Our statistics suggest that assumed background errors for tropospheric temperature are inflated (by about 30-60%), whereas there is little indication for background error inflation for stratospheric temperatures.

The use of three methods to estimate observation errors gives an indication about the reliability of the presented estimates. For most temperature-sounding channels, the methods show fairly good agreement, as length-scales for FG-errors are broad and FG-errors in radiance space are relatively small, making it possible to identify contributions from observation errors (possibly with small-scale error correlations) from FG-departure covariances. While the Desroziers diagnostic and the background error method indicate some spatial error correlations for some channels, most of these are small, such that the Hollingsworth/Lönnberg method gives similar results, even though it neglects such observation error correlations. For the humidity sounding channels, the three methods show the worst agreement. Here, the results from the Desroziers diagnostic and the background error method contradict the assumption of the Hollingsworth/Lönnberg method of spatially uncorrelated observation errors. Also, smaller length scales in the FG-errors and larger FG-errors in radiance space make contributions from observation errors less identifiable for any FG-departure-based method.

The current study makes extensive use of the Desroziers diagnostic (Desroziers et al. 2005), including for the estimation of inter-channel and spatial observation error correlations. It should be noted that the limitations and properties of this method are still an area of active research (Desroziers et al. 2009). For observations with no spatial error correlations, there is considerable evidence that the method provides reasonable estimates, in agreement with other methods (e.g., Chapnik 2009). For the majority of channels, the Desroziers diagnostic and the background error method suggest that spatial observation error correlations are indeed small with small length-scales, so we have good confidence in the results. For channels where the two methods suggest some spatial error correlations (e.g., water vapour channels or shortwave infrared temperature sounding channels) we found the results to still appear reasonable at least qualitatively. For instance, the method identifies strong spatial observation error correlations in the case of an AIRS CO channel (1875) as a result of treating CO as fixed in the observation operator, it suggests small-scale error correlations for water vapour channels for unrepresented scales, or it attributes the chessboard pattern in many IASI FG-departure covariances to observation error correlations. While these findings appear reasonable at least qualitatively, more work is required to investigate how reliable the estimates are quantitatively when observation errors have spatial error correlations that are more similar to those for background errors.

While our findings for observation errors and their inter-channel correlations for AIRS agree qualitatively well with Garand et al. (2007), there are significant differences in the observation error covariance estimates, with

Garand et al. (2007) suggesting larger errors and correlations for some channels. This highlights that the estimates are specific to the use of the radiance data in a given data assimilation system, and differences in bias correction or quality control will lead to different observation error covariance estimates for different assimilation systems.

The current observation error covariance estimates will be used to provide guidance for the specification of observation error covariances and thinning scales used in the ECMWF assimilation system. It is not expected that the estimates given here can be used directly, as other aspects may need to be taken into account, such as uncorrected residual biases (of observations and the forecast model), the performance of quality control, or limitations in the assumed background error covariances. Also, the current statistics have been derived as global means; local effects may require further refinements of observation errors. Nevertheless, the present study suggests that there is scope for an improved assimilation of some of the instruments investigated here, even with diagonal observation errors. For instance, our statistics suggest that AMSU-A may be used more densely or with smaller observation errors, given that spatial and inter-channel observation error correlations appear small and the current assimilation choices appear rather conservative. For AIRS and IASI, the choice of observation error could be harmonised and artificial steps in the assumed observation error removed. However, the situation for AIRS and IASI is otherwise more complex due to the diversity of observation error characteristics for different channels. While spatial observation error correlations appear mostly small (except for the AIRS short-wave channels), the presence of inter-channel error correlations for some channels may require to take such error correlations explicitly into account.

Acknowledgements

Mike Fisher, Marco Matricardi, Tony McNally, and Gabor Radnoti provided assistance and feedback on various aspects of the study. Discussions with James Cameron and Fiona Hilton (Met.Office), Lars Fiedler (EUMETSAT), and Denis Blumstein (CNES) on the IASI chessboard feature are also gratefully acknowledged.

References

Aumann, H., M. Chahine, C. Gautier, M. Goldberg, E. Kalnay, L. McMillin, H. Revercomb, P. Rosenkranz, W. Smith, D. Staelin, L. Strow, and J. Susskind, 2003: AIRS/AMSU/HSB in the Aqua mission: Design, science objectives, data products, and processing system. *IEEE Trans. Geosci. Remote Sens.*, **41**, 253–264.

Bormann, N., S. Kobayashi, M. Matricardi, A. McNally, B. Krzeminski, J.-N. Thépaut, and P. Bauer, 2008: Recent developments in the use of atovs data at ecmwf. In Proceedings of the 16th international TOVS study conference, Angra dos Reis, Brazil, CIMSS, University of Wisonsin, Madison, US.

Bormann, N., S. Saarinen, G. Kelly, and J.-N. Thépaut, 2003: The spatial structure of observation errors in Atmospheric Motion Vectors from geostationary satellite data. *Mon. Wea. Rev.*, **131**, 706–718.

Bormann, N., D. Salmond, M. Matricardi, A. Geer, and M. Hamrud, 2009: The RTTOV-9 upgrade for clear-sky radiance assimilation in the IFS. Technical Memorandum 586, ECMWF, Reading, UK, 26 pp [available under www.ecmwf.int/publications/library/do/references/list/14].

Chalon, G., F. Cayla, and D. Diebel, 2001: IASI: An advanced sounder for operational meteorology. In Proc. 52nd Congress of IAF, Toulouse France, 1-5 Oct. 2001, http://smsc.cnes.fr/IASI/A_publications.htm [Accessed August 2009].

Chapnik, B., 2009: On-line observation covariance matrix tuning based on optimality diagnostic. In Proceedings of the ECMWF workshop on diagnostics of data assimilation system performance, ECMWF, Reading, UK, in press.

Chapnik, B., G. Desroziers, F. Rabier, and O. Talagrand, 2006: Diagnosis and tuning of observational error in a quasi-operational data assimilation setting. *Quart. J. Roy. Meteor. Soc.*, **132**, 543–565.

Collard, A., 2007: Selection of IASI channels for use in numerical weather prediction. *Quart. J. Roy. Meteor. Soc.*, **133**, 1977–1991.

Collard, A., and A. McNally, 2009: The assimilation of Infrared Atmospheric Sounding Interferometer radiances at ECMWF. *Quart. J. Roy. Meteor. Soc.*, **135**, 1044–1058.

Dando, M., A. Thorpe, and J. Eyre, 2007: The optimal density of atmospheric sounder observations in the met.office NWP system. *Quart. J. Roy. Meteor. Soc.*, **133**, 1933–1943.

Dee, D., 2004: Variational bias correction of radiance data in the ECMWF system. In ECMWF Workshop on Assimilation of High Spectral Resolution Sounders in NWP, ECMWF, Reading, UK, 97–112.

Dee, D., and A. da Silva, 1999: Maximum-likelihood estimation of forecast and observation error covariance parameters. Part I: Methodology. *Mon. Wea. Rev.*, **127**, 1822–1834.

Desroziers, G., L. Berre, and B. Chapnik, 2009: Objective validation of data assimilation systems: Diagnosing sub-optimality. In Proceedings of the ECMWF workshop on diagnostics of data assimilation system performance, ECMWF, Reading, UK, in press.

Desroziers, G., L. Berre, B. Chapnik, and P. Poli, 2005: Diagnosis of observation, background and analysis-error statistics in observation space. *Quart. J. Roy. Meteor. Soc.*, **131**, 3385–3396.

Desroziers, G., and S. Ivanov, 2001: Diagnosis and adaptive tuning of information error parameters in a variational assimilation. *Quart. J. Roy. Meteor. Soc.*, **127**, 1433–1452.

Fisher, M., 2003: Background error covariance modelling. In Proceedings of the ECMWF Seminar on recent developments in data assimilation from atmosphere and ocean, ECMWF, Reading, UK, 45–64.

Garand, L., S. Heilliette, and M. Buehner, 2007: Interchannel error correlation associated with airs radiance observations: Inference and impact in data assimilation. *J. Appl. Meteor.*, **46**, 714–725.

Goodrum, G., K. Kidwell, and W. Winston, 2009: NOAA KLM User's Guide with NOAA-N, -N-Prime supplement. NOAA, http://www2.ncdc.noaa.gov/docs/klm/cover.htm, accessed: 17 August 2009.

Hollingsworth, A., and P. Lönnberg, 1986: The statistical structure of short-range forecast errors as determined from radiosonde data. Part I: The wind field. *Tellus*, **38A**, 111–136.

Krzeminski, B., N. Bormann, T. McNally, and P. Bauer, 2009: Revision of the hirs cloud detection. EUMETSAT/ECMWF Fellowship Programme Research Report 18, ECMWF, Reading, U.K., in press.

Liu, Z.-Q., and F. Rabier, 2003: The potential of high-density observations for numerical weather prediction: A study with simulated observations. *Quart. J. Roy. Meteor. Soc.*, **129**, 3013–3035.

McNally, A., and P. Watts, 2003: A cloud detection algorithm for high-spectral-resolution infrared sounders. *Quart. J. Roy. Meteor. Soc.*, **129**, 2411–2323.

McNally, A., P. Watts, J. Smith, R. Engelen, G. Kelly, J.-N. Thépaut, and M. Matricardi, 2006: The assimilation of AIRS radiance data at ECMWF. *Quart. J. Roy. Meteor. Soc.*, **132**, 935–957.

Ménard, R., Y. Yang, and Y. Rochon, 2009: Convergence and stability of estimated error variances derived from assimilation residuals in observation space. In Proceedings of the ECMWF workshop on diagnostics of data assimilation system performance, ECMWF, Reading, UK, in press.

Rutherford, I. D., 1972: Data assimilation by statistical interpolation of forecast error fields. *J. Atmos. Sci.*, **29**, 809–815.

Sherlock, V., 2000: Impact of RTIASI fast radiative transfer model error on IASI retrieval accuracy. Forecasting Research Technical Report 319, The Met. Office, Bracknell, U.K., 34 pp.

Stark, J., C. Donlon, M. Martin, and M. McCulloch, 2007: OSTIA: An operation, high resolution, real time, global sea surface temperature analysis system. In Proceedings of the Oceans '07 conference, Aberdeen, UK, IEEE/OES, 061214–029.

Stewart, L., J. Cameron, S. Dance, S. English, J. Eyre, and N. Nichols, 2009: Observation error correlations in IASI radiance data. Mathematics Report Series 1/2009, University of Reading, Reading, UK, 26 pp. [available from: http://www.rdg.ac.uk/maths/research/maths–report–series.aspx, accessed 26 August 2009].